Available online at www.sciencedirect.com

ScienceDirect

Geochimica et Cosmochimica Acta 200 (2017) 167–185

Geochimica et Cosmochimica Acta

www.elsevier.com/locate/gca

Isotopic composition of Mg and Fe in garnet peridotites from the Kaapvaal and Siberian cratons

Yajun An [a], Jin-Xiang Huang [b], W.L. Griffin [b], Chuanzhou Liu [c], Fang Huang [a,*]

[a] *CAS Key Laboratory of Crust-Mantle Materials and Environments, School of Earth and Space Sciences, University of Science and Technology of China, Hefei 230026, Anhui, China*

[b] *Australian Research Council Centre of Excellence for Core to Crust Fluid Systems (CCFS) and GEMOC, Macquarie University, Sydney, NSW 2109, Australia*

[c] *State Key Laboratory of Lithospheric Evolution, Institute of Geology and Geophysics, Chinese Academy of Sciences, Beijing 100029, China*

Received 4 April 2016; revised 19 November 2016; accepted in revised form 24 November 2016; Available online 7 December 2016

Abstract

We present Mg and Fe isotopic data for whole rocks and separated minerals (olivine, clinopyroxene, orthopyroxene, garnet, and phlogopite) of garnet peridotites that equilibrated at depths of 134–186 km beneath the Kaapvaal and Siberian cratons. There is no clear difference in δ^{26}Mg and δ^{56}Fe of garnet peridotites from these two cratons. δ^{26}Mg of whole rocks varies from −0.243‰ to −0.204‰ with an average of -0.225 ± 0.037‰ (2σ, $n = 19$), and δ^{56}Fe from −0.038‰ to 0.060‰ with an average of -0.003 ± 0.068‰ (2σ, $n = 19$). Both values are indistinguishable from the fertile upper mantle, indicating that there is no significant Mg-Fe isotopic difference between the shallow and deep upper mantle. The garnet peridotites from ancient cratons show δ^{26}Mg similar to komatiites and basalts, further suggesting that there is no obvious Mg isotopic fractionation during different degrees of partial melting of deep mantle peridotites and komatiite formation.

The precision of the Mg and Fe isotope data ($\leqslant \pm 0.05$‰ for δ^{26}Mg and δ^{56}Fe, 2σ) allows us to distinguish inter-mineral isotopic fractionations. Olivines are in equilibrium with opx in terms of Mg and Fe isotopes. Garnets have the lowest δ^{26}Mg and δ^{56}Fe among the coexisting mantle minerals, suggesting the dominant control of crystal structure on the Mg-Fe isotopic compositions of garnets. Elemental compositions and mineralogy suggest that clinopyroxene and garnet were produced by later metasomatic processes as they are not in chemical equilibrium with olivine or orthopyroxene. This is consistent with the isotopic disequilibrium of Mg and Fe isotopes between orthopyroxene/olivine and garnet/clinopyroxene. Combined with one sample showing slightly heavy δ^{26}Mg and much lighter δ^{56}Fe, these disequilibrium features in the garnet peridotites reveal kinetic isotopic fractionation due to Fe-Mg inter-diffusion during reaction between peridotites and percolating melts in the Kaapvaal craton.

Keywords: Garnet peridotites; Magnesium isotopes; Iron isotopes; Lithospheric mantle; Metasomatism

1. INTRODUCTION

Mg and Fe are the major elements of common upper mantle minerals. Magnesium has one valence state (2+), while Fe has two (2+ and 3+) in the mantle, depending on redox conditions. The Mg-isotope compositions of upper mantle rocks have provided information on the formation and differentiation of planetary bodies, origin and evolution of the Earth, and the global Mg cycle (e.g., Galy et al., 2000; Huang et al., 2010; Teng et al., 2010; Liu et al., 2011). The multiple valence states of iron enhance its potential for fractionation during mantle metasomatism, partial melting, fractional crystallization, and fluid

* Corresponding author.
E-mail address: fhuang@ustc.edu.cn (F. Huang).

http://dx.doi.org/10.1016/j.gca.2016.11.041
0016-7037/

exsolution (Heimann et al., 2008; Dauphas et al., 2010; Teng et al., 2011; Poitrasson et al., 2013). Combined analyses of Mg and Fe isotopic systems could provide new constraints on the formation and evolution of the upper mantle.

The oxygen fugacity in the lithospheric mantle generally decreases with depth (Woodland and Koch, 2003; Frost and McCammon, 2008; Stagno et al., 2013). Iron isotopes are sensitive to redox conditions (Polyakov and Mineev, 2000; Shahar et al., 2008; Nebel et al., 2015; Young et al., 2015); therefore, investigation of the Fe-isotope compositions of mantle rocks from different depths may provide further information on the redox effect. The cratonic lithospheric mantle has been documented to be stabilized in the Archean (Carlson et al., 2005; Lee, 2005). Due to secular cooling of the Earth, there may be systematic differences between modern peridotites from oceanic lithosphere and ancient peridotites from cratonic lithosphere, related to different degrees of melting under various P-T conditions. This raises the question of whether Mg and Fe isotopic compositions change with degree of depletion (e.g., Su et al., 2015). The lithospheric mantle beneath Archean cratons has undergone time-integrated metasomatism (e.g., Hawkesworth et al., 1990; Pearson et al., 1995b; Kobussen et al., 2009). Metasomatism by recycled carbonate materials could potentially produce mantle rocks enriched with light Mg isotopes (Brenot et al., 2008; Pogge von Strandmann, 2008; Hippler et al., 2009; Higgins and Schrag, 2010c; Yang et al., 2012). The considerable variability of δ^{56}Fe (0.87‰) in mantle rocks and minerals can result either from equilibrium isotopic fractionation or from diffusion-driven kinetic isotope effects during metasomatism in the mantle (Beard and Johnson, 2004; Weyer and Ionov, 2007; Poitrasson et al., 2013). Therefore, the isotopic signatures of Fe and Mg have the potential to trace different types of metasomatic activity in the lithospheric mantle.

Peridotite xenoliths brought up to the Earth's surface by kimberlites and/or continental basalts provide important probes to study the vertical sections of the subcontinental lithospheric mantle (SCLM). Large amounts of Fe isotope data for igneous rocks and mantle minerals have shown that Fe in the terrestrial upper mantle is isotopically heterogeneous at the bulk-rock scale (Weyer and Ionov, 2007; Dauphas et al., 2009; Williams et al., 2009; Poitrasson et al., 2013). However, it is not clear whether Mg is isotopically homogeneous through the upper mantle scale because Mg-isotope studies have mainly focused on shallow spinel peridotites (<60 km) (Teng et al., 2010a; Xiao et al., 2013) and only a few data are available on garnet peridotites from the deeper portions of the upper mantle (Teng et al., 2010). There also are no studies on the intermineral Mg isotopic fractionations between coexisting minerals in these garnet peridotites. The Mg and Fe isotopic compositions of the bulk silicate Earth (BSE) and the mechanisms governing isotopic fractionation of Mg and Fe in the mantle thus are not fully resolved.

Archean continental blocks (cratons) are the oldest and thickest domains of the Earth's lithosphere (Jordan, 1975; Boyd et al., 1985; Pearson et al., 1995a; Jaupart and Mareschal, 1999). Speculation on the composition of the mantle roots of continental cratons has been fueled by abundant chemical and petrographic data for peridotite xenoliths from the Kaapvaal craton in southern Africa, which extends approximately to the depth of 220–250 km and has been isolated from upper mantle convection since its formation (Rudnick and Nyblade, 1999; Eaton et al., 2009). Highly depleted and anhydrous compositions have enabled it to survive major tectonic processes (Poudjom Djomani et al., 2001), but a strong metasomatic imprint has made it significantly distinct from the asthenospheric mantle (Kobussen et al., 2008b; O'Reilly and Griffin, 2010). In this study, most peridotite xenoliths extracted from Kaapvaal craton kimberlites give Archean Re-depletion model ages without clear trend between the age and the depth of origin (Carlson et al., 2000; Griffin et al., 2004b; Walker et al., 1989; Pearson et al., 1995a). In order to address the regional differences and better constrain the Mg-Fe isotopic compositions of the deep lithospheric mantle, we also have analyzed garnet lherzolites from the Udachnaya kimberlite in the central Siberian craton; this kimberlite hosts abundant peridotite xenoliths (Boyd et al., 1997; Ionov et al., 2010; Agashev et al., 2013). Garnet peridotites from the Udachnaya kimberlite have many similarities to the peridotites from the Kaapvaal craton in terms of bulk compositions, mineralogy, ages, and metasomatic histories (Boyd et al., 1997).

Here, we present combined Mg and Fe isotopic data for whole-rocks and mineral separates, including olivine, clinopyroxene (cpx), orthopyroxene (opx), garnet and phlogopite, in well-characterized garnet lherzolites and harzburgites from the Kaapvaal and Siberian cratons. The major objective of this study is to outline the Mg and Fe isotopic compositions of mantle rocks equilibrated at greater depths (134–186 km) and to broaden our understanding of compositions and evolution in the deep upper mantle represented by peridotites from the garnet stability field.

2. GEOLOGICAL BACKGROUND AND SAMPLE DESCRIPTION

2.1. Geological background

The Kaapvaal craton in southern Africa is composed of four distinct geological terrains, which were assembled between 3.7 and 2.6 Ga (de Wit et al., 1992; Carlson et al., 2000). Previous studies on peridotitic garnet xenocrysts and xenoliths have demonstrated that the SCLM under the Kaapvaal craton has experienced a series of modification processes including heating, refertilization, and thinning (Kobussen et al., 2008a; Sleep, 2003).

Previous studies on the lateral and vertical variations of the mantle structure of Siberian platform have shown that a layering exists in the SCLM beneath Udachnaya and other Siberian kimberlite pipes (Ashchepkov et al., 2008; Ashchepkov et al., 2010; Boyd et al., 1997; Griffin et al., 1999b, 2005; Nimis et al., 2009). For example, the garnets from kimberlite heavy mineral separates show an increasing depletion of the lower part of the mantle lithosphere northward (Griffin et al., 1999b). A wide variety of metasomatic modification within mantle columns can be detected at the macro and micro scales (e.g., zonation in minor and major components of cratonic mantle xenoliths) (Misra et al., 2004; Shatsky et al., 2008).

2.2. Sample description

8 of 20 peridotites in this study were sampled from the Kaapvaal craton. Seven of the eight Kaapvaal samples are from the Letseng-le-Terai (samples LT98/-) kimberlite pipe in northern Lesotho, which erupted at ~90 Ma (Woolley et al., 1996). One sample (JGF-98/6) is from the Jagersfontein kimberlite pipe, Orange Free State, South Africa, which erupted 85.6 ± 1 m.y. ago (Smith et al., 1985).

Photomicrographs of representative xenoliths from the Kaapvaal craton are shown in Fig. 1. Peridotites are mainly cpx-poor garnet-facies lherzolites and harzburgites grouped into coarse (Fig. 1a–f) and porphyroclastic (Fig. 1g and h) textural types. They mainly consist of olivine, opx, cpx, garnet and phlogopite. A detailed description can be found in the Appendix. Grain boundaries between olivine and opx are smoothly curved (Fig. 1a and b), indicating textural equilibrium among these two phases, whereas the microstructural habit of cpx (interstitial or spatially associated with garnet) suggests that it crystallized from infiltrating metasomatic melts. The garnets occur in polygranular clots with abundant inclusions of olivine and pyroxene; this texture is not necessarily primary and might reflect recrystallization (Fig. 1d). The deformed peridotite (LT98/13) is very fresh, containing small amounts of anhedral olivine, opx neoblasts, and sub-grains around coarse prophyroblasts. Sample JGF-98/6 (Jagersfontein) contains abundant phlogopite (~5%), representing an extreme example of the metasomatic process. In these garnet peridotites, textural relationships, including veins of cpx or spatial associations with phlogopite in microfractures and pockets, highlight the obvious metasomatic overprinting.

12 fresh garnet peridotites are from Udachnaya-East kimberlite pipe in Siberian platform. The kimberlites in this pipe erupted at ~360 Ma through the Daldyn block of the Siberian craton (Rosen et al., 1994). The xenoliths in this study are mainly fresh garnet lherzolites from the Udachnaya kimberlite. The Udachnaya xenoliths represent a complete range in terms of equilibration P-T (2.6–6.8 GPa, 860–1340 °C), textures (granular vs. deformed), and the modal and chemical compositions (e.g., cpx-free/cpx-bearing harzburgites to low-cpx (5–6%) lherzolites) of the lithospheric mantle in the central Siberian craton (Boyd et al., 1997; Ionov et al., 2010, 2013, 2015). They are also similar to rocks described by previous studies (Ionov et al., 2010; Bascou et al., 2011; Goncharov et al., 2012; Yaxley et al., 2012; Doucet et al., 2014).

3. ANALYTICAL METHODS

3.1. Major and trace elements

Mineral separates in peridotite xenoliths from the Kaapvaal craton were analyzed for major and trace elements by electron probe microanalyzer (EPMA) and laser-ablation (LA) ICP-MS at the University of Science and Technology of China (USTC) in grain mounts and polished sections, respectively. The detailed operation information is given in He et al. (2016). The Agilent 7700a ICP-MS instrument is coupled with an Excimer 193 nm Resonetics M-50E ATL operated at 7 Hz, 6 mJ cm^{-2} pulse energy, and 70–100 μm beam size. Helium was used as the carrier gas. Acquisition time was 90 s for background and 60 s for each signal. The sum of all measured metal oxides was normalized to 100% m/m after subtracting the loss on ignition (Halicz and Gunther, 2004; Guillong et al., 2005; Liu et al., 2008; Zhu et al., 2013; He et al., 2016). Reference sample SRM NIST 612 was used as an external standard. Three USGS basalt glass reference materials (BHVO-2G, BCR-2G, and BIR-1G) were used for calibration, which can provide more precise and accurate elemental concentrations than only using NIST SRM 610. The sequence of analysis began with four analyses of reference glasses (NIST SRM 610, BHVO-2G, BCR-2G, and BIR-1G), followed by analyses of samples and then four analyses of reference glasses again. NIST SRM 610 was repetitively analyzed every 8 samples for time-drift correction. ICPMS-DataCal software was used to perform the offline selection and integration of background and ablation signals, time-drift correction, and quantitative calibration (Liu et al., 2008). Obviously altered regions and any small secondary minerals were avoided during picking of mineral separates. An average of six separate grains per sample was used to determine the major- and trace-element compositions of the constituent minerals.

3.2. Mg and Fe isotope analyses

The mineral separates of olivine, opx, cpx, garnet, phlogopite, and whole rock powders of samples from the Kaapvaal craton were prepared for Mg- and Fe-isotope analyses. In order to exclude effects of pervasive alteration (such as serpentinization and kelyphitization), individual grains used for isotope analysis were hand-picked under a binocular microscope. To avoid kelyphitization, garnet grains without any visible discoloration or surface pitting were used. The separates were subjected to successive ultrasonic cleaning in ultrapure water to eliminate any surface contamination. Additionally, the rock powders of samples from the Siberian craton were analyzed for Mg and Fe isotopic compositions.

Isotopic ratios of Mg and Fe were measured at the USTC, following the procedure described in previous studies (Huang et al., 2011; An et al., 2014). A detailed description of the analytical procedures used for Mg and Fe separation is given in the Appendix. Total procedural blanks for Mg and Fe were less than 10 ng, which is insignificant relative to the amount of Mg and Fe put through chemical purification ($\geqslant$20 μg). Repeated analyses of whole-rock powders and mineral grains show excellent consistency of Mg and Fe isotope data. Seven USGS whole-rock standards (RGM-2, GA, GS-N, AGV-2, BCR-2, DTS-1, and PCC-1) were measured for δ^{26}Mg and δ^{56}Fe, respectively. Three in-house pure Mg solution

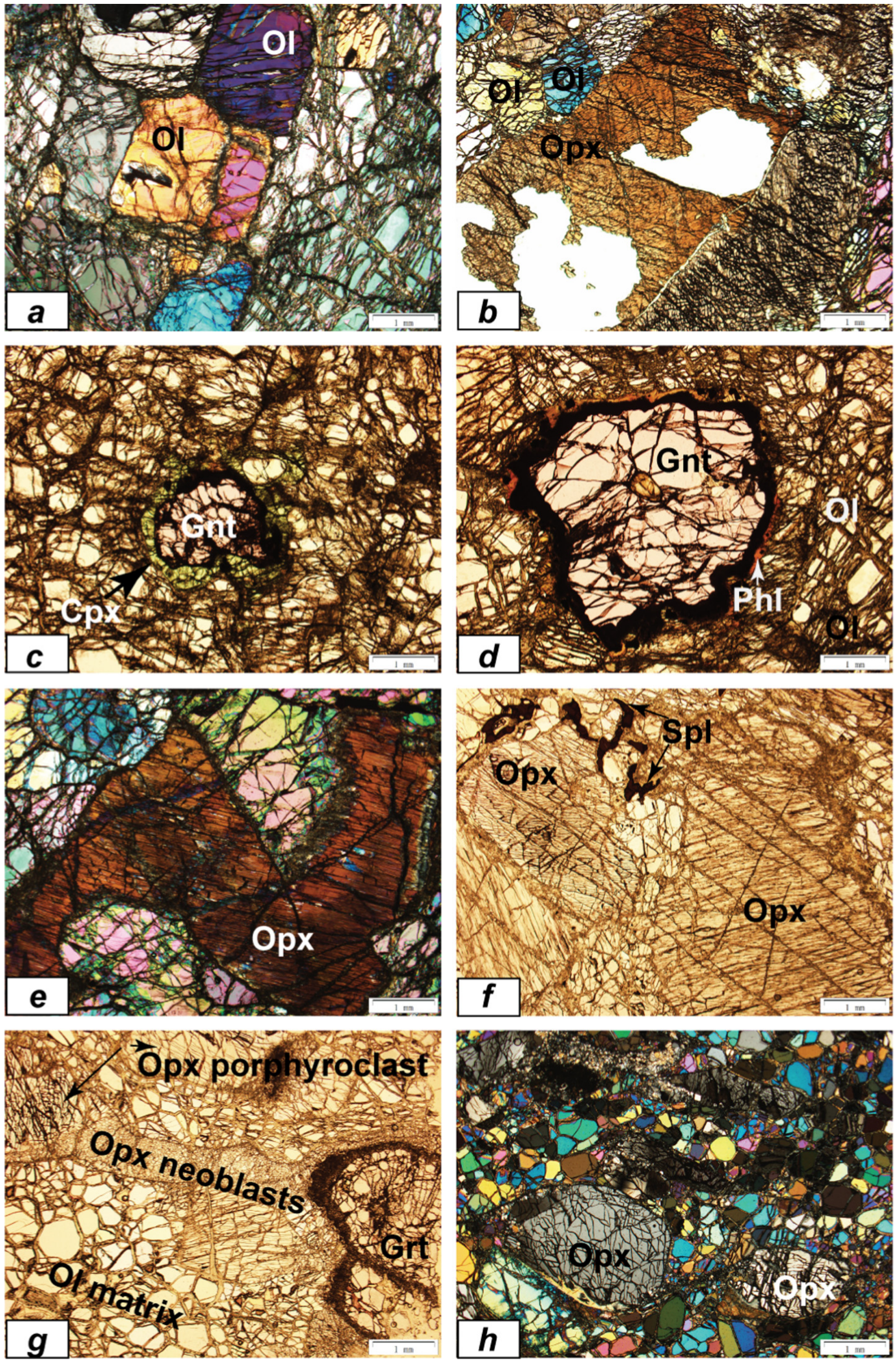

Fig. 1. Garnet peridotites from the Kaapvaal craton under transmitted cross-polarized (a, b, e, and h) and plane-polarized light (c, d, f, and g) show granular (a–f) and mosaic-porphyroclastic (g and h) textures. Ol, olivine; Opx, orthopyroxene; Cpx, clinopyroxene; Spl, spinel. Garnets (Gnt) are mainly round or ellipsoidal, often with rounded inclusions of olivine and opx (d). The dark rim around garnet porphyroclasts is 'kelyphite' (c, d, and g). Coarse, texturally equilibrated olivine and opx commonly show triple junctions at 120° in a microstructure transitional to mosaic equigranular (a, b). Cpx occurs as smaller subhedral or irregularly shaped crystals, often on garnet rims (c). Note that spinel in sample JGF-98/6 is usually inter-grown with opx (f) and probably exsolved from high-T opx on cooling, or formed during breakdown of pre-existing garnet due to a decrease in pressure. Opx also occurs as lobate grains that may embay olivine, showing thin exsolution lamellae of garnet and diopside (e). In the left side of Fig. 1g, a large opx porphyroclast is recrystallized into a band of fine-grained neoblasts, while garnets are slightly elongated, parallel to the opx lineation. Recrystallized opx porphyroclasts and coarser-grained polygonal strain-free olivine neoblasts can be seen in the fluidal mosaic peridotite LT98/13 (h).

standards (CAM-1, SRM980, and IGGMg1), and two in-house pure Fe solution standards (UIFe and GSB-1) were routinely analyzed (Table S1). These data show excellent agreement with literature values, highlighting the reliability of the Mg and Fe isotope data.

4. RESULTS

Major- and trace-element compositions of minerals from Kaapvaal peridotites are reported in the Appendix (Table S2). Magnesium and iron isotopic compositions of bulk peridotites from both Kaapvaal and Siberian cratons and minerals separates from Kaapvaal craton (olivine, cpx, opx, garnet, and phlogopite) are listed in Tables 1 and 2.

4.1. Major elements

The minerals have homogeneous major and trace element compositions and no compositional zoning has been found. The average compositions of multiple analyses are given in the Appendix (Table S2). The major and trace element data obtained by EMPA and LA-ICP-MS for individual minerals are similar within the respective uncertainties, indicating the homogeneity of the mineral separates and the robustness of our data (Table S2). The temperatures and pressures of the last equilibration of peridotite xenoliths from the Kaapvaal craton are 990–1372 °C and 4.2–5.34 GPa, respectively (Fig. 2). At a given pressure, most thermobarometers provide identical temperatures within the uncertainty (Table 3) (Ashchepkov, 2006; Brey et al., 2008; Brey and Köhler, 1990; Canil, 1994, 1999; Carswell, 1991; Finnerty and Boyd, 1987; Nickel and Green, 1985; Nimis and Grütter, 2010; Putirka, 2008; Ryan et al., 1996; Wu and Zhao, 2007), except a few discrepancies which may be attributed to the effect of Fe^{3+} in the garnets for Fe-Mg exchange thermometers (Harley, 1984; Griffin et al., 1989b; O'Neill and Wood, 1979; Krogh, 1988).

Most samples from the Kaapvaal craton in this study have highly depleted major-element compositions with FeO of 5.83–6.84 wt.%, CaO of 0.39–0.89 wt.%, Al_2O_3 of 0.83–1.55 wt.%, TiO_2 of 0.02–0.08 wt.%, Na_2O <0.07 wt.% and K_2O of 0.02–0.07 wt.% (Griffin et al., 2004b). $Mg^{\#}$ of olivine is high, 92.4 ± 2.4, indicative of large degrees (>30–50%) of melt extraction at high pressures (Fig. S1) (>5 GPa). The phlogopite-bearing sample JGF-98/6 from Jagersfontein has higher TiO_2 (0.31 wt.%) and K_2O (0.42 wt.%) contents. The refractory nature of most peridotite xenoliths is also indicated by high $Mg^{\#}$ in the constituent minerals: $Mg^{\#}_{opx} = 92.9–93.7$, $Mg^{\#}_{cpx} = 91.7–92.0$, and $Mg^{\#}_{garnet} = 83.7–85.7$, with the exception of sample LT98/13, $Mg^{\#}_{opx} = 91.4$, $Mg^{\#}_{cpx} = 89.7$, and $Mg^{\#}_{garnet} = 84.4$.

Red to lilac chrome-pyrope garnet crystals with sizes up to a few millimeters are abundant in the coarse peridotites, while garnets in the sheared peridotite xenoliths (LT98/13) are dark red, reflecting the high FeO contents (7.11 wt.%). In general, garnets are quite homogeneous except for the outer ~100 μm rim in contact with the kelyphite with variable Cr, Ti, Ca, Mg, and Fe concentrations (Griffin et al., 1996).

4.2. Trace elements

Garnets can be divided into two groups based on their REE patterns (Fig. S2). The first group has sinusoidal REE patterns, a usual feature of harzburgitic (low CaO) garnets included in diamonds (Stachel and Harris, 2008). The second group has a flat REE pattern from MREE to HREE, and a sharp decrease from Nd to La, which is common for garnet megacrysts and high-T lherzolites (Burgess and Harte, 2004). Shimizu (1975) observed that the sinusoidal garnet REE patterns are typical for coarse (low-T) peridotites, whereas normal REE patterns characterize the sheared (high-T) peridotites. The sinusoidal REE patterns of the garnet cores are regarded as "primary" features reflecting an ancient metasomatic event superimposed on a depleted protolith (Griffin et al., 1999d). This is consistent with the ancient (>1 Ga) enrichment event that was identified by Stiefenhofer (1993) using Sm-Nd isotope systematics.

All cpx grains from coarse garnet peridotites have similar LREE-enriched chondrite-normalized REE patterns with a maximum defined by Nd (Fig. S2). The cpx in sample LT98/13 is enriched in LREE with a maxima at Ce-Nd in their REE patterns, a typical feature in deformed peridotites (Pearson et al., 2003). The trace element patterns show deep negative Ti and slight negative Zr anomalies (Fig. S2).

4.3. Mg isotopes

$\delta^{26}Mg$ of bulk peridotites from both Kaapvaal and Siberian cratons are given in Table 1 and those of mineral separates (olivine, opx, cpx, garnet, and phlogopite) from Kaapvaal peridotites are shown in Table 2. $\delta^{26}Mg$ of olivine from the Northern Lesotho peridotite xenoliths varies from −0.269‰ to −0.211‰, opx from −0.247‰ to −0.209‰, cpx from −0.292‰ to −0.225‰, and garnet from −0.718‰ to −0.517‰ (Table 2). The average of $\delta^{26}Mg$ of olivine is $-0.236 \pm 0.042‰$ (2σ, $n = 7$), opx is $-0.230 \pm 0.024‰$ (2σ, $n = 7$), cpx is $-0.255 \pm 0.057‰$ (2σ, $n = 4$), and garnet is $-0.649 \pm 0.138‰$ (2σ, $n = 7$). The phlogopite from sample LT98/5 has slightly higher $\delta^{26}Mg$ ($-0.118 \pm 0.037‰$) than the coexisting olivine. Olivine and opx separates from the Jagersfontein sample (JGF-98/6) are characterized by slightly heavier $\delta^{26}Mg$ ($-0.142 \pm 0.030‰$ and $-0.094 \pm 0.054‰$, respectively).

$\Delta^{26}Mg_{olivine\text{-}opx}$ of samples from Kaapvaal craton varies from 0.022‰ to −0.072‰ with an average of $-0.019 \pm 0.065‰$ (2σ), while $\Delta^{26}Mg_{olivine\text{-}cpx}$ of 4 samples varies from 0.052‰ to −0.027‰ with an average of $0.022 \pm 0.070‰$ (2σ) (Table 4). $\Delta^{26}Mg_{olivine\text{-}garnet}$ of 7 samples varies from 0.497‰ to 0.299‰ with an average of $0.411 \pm 0.158‰$ (2σ), while $\Delta^{26}Mg_{opx\text{-}garnet}$ varies from 0.282‰ to 0.487‰ with an average of $0.418 \pm 0.144‰$ (2σ) (Table 4). The $\delta^{26}Mg$ of bulk peridotites from the Kaapvaal craton varies from −0.236‰ to −0.210‰ with an average of $-0.221 \pm 0.034‰$ (2σ, $n = 7$), and that of garnet lherzolites from Siberian craton varies from −0.243‰ to −0.204‰, with an average of $-0.230 \pm 0.039‰$ (2σ, $n = 12$), showing no resolvable discrepancy between the $\delta^{26}Mg$ of garnet peridotites from these two areas (Fig. 3).

Table 1
Mg-Fe isotopic compositions of garnet peridotites from the Kaapvaal and Siberian cratons.

	Sample	Rock type	MgO	FeO	δ^{26}Mg	2SD	δ^{25}Mg	2SD	N	δ^{56}Fe	2SD	δ^{57}Fe	2SD	N
Kaapvaal Craton	LT98/3	Coarse garnet lherzolite			−0.236	0.015	−0.119	0.019	4	0.060	0.034	0.062	0.072	4
	LT98/5	Coarse garnet lherzolite	41.33	5.83	−0.210	0.013	−0.108	0.044	4	0.022	0.032	0.002	0.083	4
		Replicate			−0.214	0.022	−0.114	0.031	8	0.026	0.029	0.047	0.019	4
	LT98/10	Coarse garnet harzburgite	42.39	6.79	−0.234	0.035	−0.133	0.006	4	−0.038	0.038	−0.038	0.065	12
	LT98/12	Coarse garnet harzburgite	43.44	6.07	−0.211	0.039	−0.106	0.035	8	0.005	0.042	0.021	0.087	4
	LT98/13	Foliated garnet lherzolite	42.25	7.75	−0.216	0.025	−0.112	0.015	4	0.032	0.022	0.058	0.036	4
	LT98-14	Coarse garnet lherzolite	43.12	5.97	−0.228	0.045	−0.119	0.027	8	0.019	0.044	0.022	0.075	20
	LT98/15	Depl coarse garnet lherzolite	43.40	6.06	−0.226	0.022	−0.123	0.035	8	−0.034	0.050	−0.041	0.106	12
		Kaapvaal av.			**−0.221**	**0.034**	**−0.116**	**0.032**	**40**	**0.007**	**0.062**	**0.012**	**0.085**	**57**
	JGF98/6	Coarse garnet harzburgite	42.48	6.84	−0.168	0.020	−0.080	0.030	8	−0.309	0.014	−0.449	0.028	4
		Replicate			−0.162	0.035	−0.078	0.022	8	−0.300	0.021	−0.415	0.039	4
Siberian Craton	UD01-248		41.92	8.33	−0.242	0.007	−0.135	0.048	3	−0.009	0.039	−0.020	0.063	3
	UD01-287		43.45	8.56	−0.234	0.059	−0.120	0.012	3	−0.037	0.030	−0.002	0.125	3
	UD01-288		38.09	11.87	−0.242	0.042	−0.130	0.034	6	0.025	0.035	0.041	0.075	6
	UD01-299		44.05	8.64	−0.228	0.040	−0.116	0.023	3	0.001	0.031	0.015	0.076	3
	UD01-338		42.15	7.91	−0.228	0.048	−0.115	0.020	3	−0.021	0.040	−0.038	0.080	6
	UD02-01		43.69	8.87	−0.218	0.039	−0.122	0.024	4	−0.062	0.026	−0.120	0.058	3
	UD03-57		44.57	8.76	−0.232	0.032	−0.132	0.023	4	−0.019	0.009	−0.037	0.034	3
	UD04-01		45.23	8.73	−0.233	0.021	−0.105	0.040	3	−0.027	0.045	−0.016	0.087	3
	UD04-56		40.35	9.45	−0.243	0.068	−0.129	0.059	3	0.032	0.042	0.035	0.128	3
	UD04-59		43.66	9.99	−0.237	0.048	−0.121	0.040	6	0.023	0.008	0.056	0.060	3
	UD04-108		43.70	8.64	−0.211	0.013	−0.097	0.030	3	−0.069	0.036	−0.111	0.092	3
	UD04-113		42.68	9.29	−0.204	0.047	−0.100	0.030	4	−0.067	0.028	−0.070	0.026	3
		Siberian av.			**−0.230**	**0.039**	**−0.119**	**0.035**	**43**	**−0.010**	**0.065**	**−0.008**	**0.112**	**38**
	Total WR Av.				**−0.225**	**0.037**	**−0.118**	**0.033**	**91**	**−0.003**	**0.068**	**−0.001**	**0.108**	**100**

Bold values represent the average values of whole rocks for garnet peridotites from the Kaapvaal craton, Siberian craton and both of these two cratons, repectively.

Table 2
Mg-Fe isotopic compositions for mantle minerals from the Kaapvaal craton.

Sample	Mineral	MgO	FeO	$\delta^{26}Mg$	2SD	$\delta^{25}Mg$	2SD	N	$\delta^{56}Fe$	2SD	$\delta^{57}Fe$	2SD	N
LT98/3	Olivine	49.72	7.69	−0.252	0.030	−0.120	0.021	4	0.062	0.035	0.085	0.054	8
	Opx	34.93	4.65	−0.233	0.034	−0.136	0.030	4	0.045	0.040	0.090	0.048	4
	Cpx	16.84	2.73	−0.225	0.024	−0.111	0.022	4	0.020	0.044	0.057	0.079	12
	Garnet	20.21	6.92	−0.662	0.042	−0.343	0.041	8	−0.088	0.030	−0.098	0.088	8
LT98/5	Olivine	50.08	7.46	−0.220	0.036	−0.124	0.009	4	0.072	0.012	0.104	0.082	4
	Opx	35.01	4.46	−0.222	0.017	−0.116	0.035	4	0.034	0.038	0.078	0.112	4
	Replicate			−0.238	0.025	−0.117	0.044	4	0.025	0.017	0.018	0.083	4
	Cpx	16.77	2.64	−0.243	0.006	−0.128	0.018	5	−0.012	0.017	−0.009	0.040	4
	*after Mg column;								−0.012	0.018	−0.055	0.109	3
	Garnet	20.45	6.55	−0.718	0.037	−0.366	0.028	8	−0.033	0.040	−0.070	0.065	8
	Replicate			−0.716	0.037	−0.348	0.012	4	−0.021	0.029	−0.042	0.077	4
	Phlogopite	26.05		−0.118	0.037	−0.074	0.020	4	0.022	0.068	0.053	0.071	4
LT98/10	Olivine	50.09	8.09	−0.269	0.028	−0.121	0.007	4	−0.013	0.034	−0.020	0.048	4
	Opx	35.04	4.74	−0.220	0.042	−0.114	0.042	8	−0.024	0.034	−0.034	0.108	4
	Garnet	19.39	6.67	−0.593	0.028	−0.305	0.049	4	−0.067	0.014	−0.107	0.034	4
	Replicate			−0.582	0.043	−0.298	0.026	8	−0.070	0.026	−0.111	0.036	4
LT98/12	Olivine	50.71	7.14	−0.241	0.038	−0.123	0.034	8	0.011	0.034	0.024	0.119	4
	Opx	35.10	4.21	−0.247	0.018	−0.134	0.023	4	−0.003	0.024	−0.002	0.072	4
	Garnet	20.78	5.93	−0.687	0.041	−0.358	0.025	8	−0.040	0.041	−0.031	0.078	3
LT98/13	Olivine	48.95	9.36	−0.218	0.029	−0.107	0.024	4	0.006	0.028	0.023	0.075	8
	Opx	32.81	5.54	−0.235	0.020	−0.119	0.016	4	0.018	0.044	0.010	0.082	4
	Cpx	20.02	4.09	−0.259	0.026	−0.133	0.015	4	0.001	0.037	0.022	0.073	8
	Garnet	21.05	7.09	−0.517	0.047	−0.279	0.029	8	−0.019	0.030	−0.044	0.055	4
LT98-14	Olivine	50.24	7.18	−0.211	0.037	−0.107	0.030	4	0.008	0.032	0.031	0.047	8
	Opx	34.89	4.43	−0.233	0.030	−0.117	0.022	16	−0.006	0.044	−0.033	0.074	16
	Garnet	19.90	6.73	−0.673	0.042	−0.349	0.032	4	−0.092	0.010	−0.127	0.029	4
LT98/15	Olivine	50.37	7.32	−0.241	0.018	−0.127	0.023	4	−0.015	0.025	−0.027	0.079	4
	Opx	35.01	4.58	−0.209	0.014	−0.096	0.028	4	−0.005	0.018	−0.100	0.021	4
	Cpx	15.94	2.47	−0.292	0.033	−0.145	0.026	4	−0.063	0.014	−0.075	0.107	4
	Garnet	20.08	6.73	−0.691	0.017	−0.353	0.030	4	−0.075	0.049	−0.126	0.062	8
JGF98/6	Olivine	50.68	7.47	−0.139	0.009	−0.075	0.018	4	−0.395	0.025	−0.562	0.050	4
	Replicate			−0.145	0.044	−0.072	0.023	4	−0.378	0.008	−0.582	0.023	4
	Opx	36.28	4.96	−0.073	0.031	−0.047	0.022	8	−0.390	0.035	−0.567	0.024	4
	Replicate			−0.114	0.035	−0.061	0.033	8	−0.380	0.024	−0.537	0.079	4

N stands for the number of repeated analyses of the same solution by MC-ICP-MS.

4.4. Fe isotopes

$\delta^{56}Fe$ of bulk peridotites are listed in Table 1 and the data for mineral separates from Kaapvaal peridotites are listed in Table 2. $\delta^{56}Fe$ in olivine from the Northern Lesotho peridotites varies from −0.015‰ to +0.072‰ with an average of +0.019 ± 0.069‰ (2σ, $n = 7$), opx from −0.024‰ to +0.045‰ with an average of +0.010 ± 0.047‰ (2σ, $n = 7$), and cpx from −0.063‰ to +0.020‰ with an average of −0.013 ± 0.061‰ (2σ, $n = 4$). $\delta^{56}Fe$ of garnet ranges from −0.092‰ to −0.019‰, with an average of −0.060 ± 0.053‰ (2σ, $n = 7$). The phlogopite from sample LT98/5 has a $\delta^{56}Fe$ of 0.022 ± 0.068‰ (2σ, $n = 1$). Unusually, olivine and opx of the Jagersfontein sample (JGF-98/6) have low $\delta^{56}Fe$ (−0.386 ± 0.025‰ and −0.385 ± 0.030‰, respectively) relative to the other samples.

$\Delta^{56}Fe_{olivine\text{-}opx}$ of all samples varies from 0.047‰ to −0.015‰ with an average of 0.009 ± 0.038‰ (2σ), and $\Delta^{56}Fe_{olivine\text{-}cpx}$ of 4 samples varies from 0.084‰ to 0.004‰ with an average of 0.052 ± 0.066‰ (2σ) (Table 4). $\Delta^{56}Fe_{olivine\text{-}garnet}$ of 7 samples varies from 0.150‰ to 0.024‰ with an average of 0.075 ± 0.080‰ (2σ). $\Delta^{56}Fe_{opx\text{-}garnet}$ varies from 0.037‰ to 0.132‰ with an average of 0.066 ± 0.068‰ (2σ).

The Kaapvaal peridotites display a range of $\delta^{56}Fe$ from −0.038 ± 0.038‰ to 0.060 ± 0.034‰ with an average of 0.007 ± 0.062‰ (2σ, $n = 7$) (Fig. 4), and the garnet lherzolites from the Siberian craton vary from −0.069 ± 0.036‰ to 0.032 ± 0.042‰ with an average of −0.010 ± 0.065‰ (2σ, $n = 12$). This is consistent with the published $\delta^{56}Fe$ values (from −0.54‰ to +0.19‰) of other mantle peridotite xenoliths (Craddock et al., 2013; Poitrasson et al., 2013; Schoenberg and Blanckenburg, 2006; Weyer et al., 2005; Williams et al., 2005; Weyer and Ionov, 2007; Zhao et al., 2015). The calculated $\delta^{26}Mg$ and $\delta^{56}Fe$ of the bulk peridotites (based on the modes of olivine, opx, cpx, and garnet) are consistent with the measured values within uncertainties (Table S3 in the Appendix).

5. DISCUSSION

5.1. Metasomatism in the SCLM of the Kaapvaal craton

The whole-rock analyses of peridotite xenoliths from the Kaapvaal craton in this study show enriched trace-element

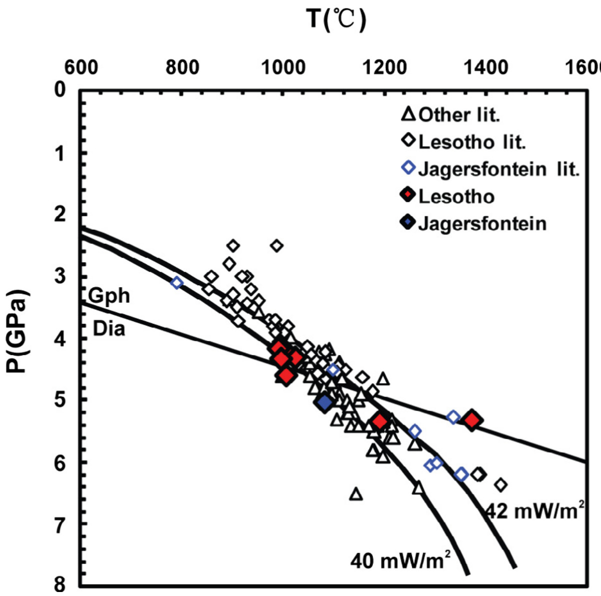

Fig. 2. Estimates of P-T equilibrium conditions of Kaapvaal peridotite xenoliths. Red diamonds are Lesotho peridotites from this study and blue ones are Jagersfontein peridotite; open symbols represent literature data for xenoliths from group I kimberlites (Kimberley, Lesotho, Jagersfontein, Frank Smith –(Simon et al., 2003)). The graphite/diamond transition line is shown. Nearly all Kaapvaal samples are plotted between the 40 and 42 mW/m^2 conductive geotherms of Chapman and Pollack (1977). Equilibration pressures and temperatures are also similar to other cratonic xenoliths, close to a 44 mW/m^2 geotherm. (For interpretation of the references to colour in this figure legend, the reader is referred to the web version of this article.)

compositions (e.g., LREE enrichment); these features, together with the occurrence of phlogopite and veined cpx, suggest that the SCLM was affected by multistage distinct metasomatic episodes, consistent with previous studies (Kelemen et al., 1998; Simon et al., 2007; Wasch et al., 2009). The increasing extent of melt-related metasomatism with depth (Griffin et al., 2003a) is also shown in the geochemical characteristics of the deformed peridotites (e.g., higher FeO) (O'Reilly and Griffin, 2010).

The investigated Lesotho garnet peridotites fall within the Type 1 mantle lherzolites defined by the trace-element compositions of cpx (Grégoire et al., 2003), which display characteristics almost identical to those of the modally metasomatized PIC (Phlogopite- Ilmenite-Cpx rocks (Grégoire et al., 2002) (Fig. S3). Combined with the petrographic characteristics, this indicates that all cpx analyzed in this study is probably secondary. Chondrite-normalized REE patterns of garnets range from sinusoidal to LREE depleted-HREE enriched shapes (Fig. S3), likely reflecting garnet-melt equilibrium during the interaction of peridotites with differentiated melts in the mantle (Burgess and Harte, 2004; Stachel et al., 2004). Garnets from shallow harzburgites have highly fractionated REE compositions, whereas high-pressure lherzolites close to the base of the lithosphere tend to have garnets with normal LREE depleted-HREE enriched patterns.

We have compared REE distribution coefficients for cpx/garnet ($^{cpx/garnet}D$) (Fig. 5) with the experimentally-determined values in the literature (Shannon, 1976; Green et al., 2000; Van Achterbergh et al., 2001). This comparison shows that cpx and garnets from the coarse peridotites are definitely not in HREE equilibrium, while the REE partitioning relationships for the high-T peridotite are consistent with equilibrium (Fig. 5). It is possibly due to that metasomatising melts can easily modify the more incompatible LREE of primary minerals, but the HREEs were not completely re-equilibrated due to their high abundances.

5.2. Inter-mineral Mg and Fe isotopic fractionations

5.2.1. Inter-mineral Mg isotopic fractionation

Magnesium-isotope data for mantle minerals in this study are shown in Fig. 6. The small isotopic offsets between olivine and opx are consistent with the observations from spinel peridotites in other studies (Handler et al., 2009; Yang et al., 2009; Young et al., 2009). They are also broadly consistent with theoretical prediction for inter-mineral equilibrium fractionations at high temperature (Young et al., 2009; Schauble, 2011; Huang et al., 2013) (Fig. 6), indicating that Mg isotopes are in equilibrium between olivine and opx at a hand sample scale. However, the Mg isotopic fractionations between garnet and other minerals (olivine/opx/cpx) differ distinctly from the theoretical prediction for equilibrium inter-mineral fractionation (Fig. 6 and Fig. S4). Given the temperature and pressure conditions ($T = 990$–1372 °C, $P = 4.2$–5.31 GPa), the equilibrium Mg isotopic fractionation between olivine and garnet in this study can be up to 0.5‰, about 10 times of the uncertainty of our Mg isotope analyses. Garnet has lighter δ^{26}Mg than other minerals, as observed in eclogites (Li et al., 2011; Huang et al., 2016). In this study, there is a decreasing extent of Mg isotopic fractionation between garnet and olivine/opx with increasing depth (Fig. 7), probably reflecting the effect of increasing temperature (from 990 °C to 1372 °C) with depth (138 km ~180 km *vs* $P = 4.16$ GPa–5.34 GPa). The measured $\Delta^{26}Mg_{olivine\text{-}garnet}$ (0.299 ± 0.051‰ to 0.497 ± 0.046‰) and $\Delta^{26}Mg_{opx\text{-}garne}$ (0.282 ± 0.047‰ to 0.487 ± 0.042‰) are not consistent with theoretical calculations, 0.535‰–1.001‰ and 0.600‰–1.118‰, respectively (Huang et al., 2013) (dashed line in Fig. 7), suggesting isotopic disequilibrium between garnet and other minerals, in line with the elemental and mineralogical features of the garnet.

As mentioned above, most of the garnet and cpx in Kaapvaal xenoliths appear to be secondary products of post-melting metasomatism (Shimizu et al., 1997; Simon et al., 2003). The sheared peridotites represent ancient coarsely-granular rocks that underwent extensive dynamic and static recrystallization of opx and olivine (Skemer and Karato, 2008; Baptiste et al., 2012). The high temperatures recorded by these lherzolites in cratonic settings suggest a thermal perturbation, consistent with the intrusion of mafic melts (Bell et al., 2003; Kobussen et al., 2009; Lazarov et al., 2009b). However, this thermal process was transient as evidenced in the studies on zoned garnets from sheared lherzolites (Griffin et al., 1996), and could not

Table 3
The calculated temperatures (°C) and pressures (kbar) for garnet peridotites from the Kaapvaal craton.

Sample	LT98/3	LT98/5	LT98/10	LT98/12	LT98/13	LT98/14	LT98/15	Accuracy	Reference
T	1025	1002	1191	990	1372	1007	995	±60	(1)
$T^{ca\text{-}in\text{-}Opx}{}_{corr}$	1016	990	1193	976	1357	995	981		(2)
$T_{Ca\text{-}in\text{-}Opx}$	1018	1007	1125	994	1225	1016	999		(3)
$T_{Ni\text{-}in\text{-}gnt}$	1042	1038	1138	1021	1326	1030	1032		(4)
T_{Ni}	1049	1055	1194	1012	1531	1007	1013	±50	(5)
T_{Ni}	1048	1044	1130	1030	1287	1037	1039		(6)
T_{Ni}	1110	1116	1269	1070	1645	1064	1071		(7)
$T_{Fe\text{-}Mg}$	1023	1033	1110	1002	1283	1023	1030	±92	(8)
T_{NG09}	1067	1075	1225	1037	1413	1082	1080		(2)
$T_{Fe\text{-}Mg}$	1317	1368	1570	1303	1701	1270	1286	±60	(9)
$T_{Fe\text{-}Mg}$	1048	1073	1165	1045	1279	1030	1030		(10)
$T_{Fe\text{-}Mg}$	1110	1150	1469	1154	1495	1184	1283		(11)
T_{BKN}	1095	1101	1237		1425		1036	±30	(12)
T	923	915			1276		1008	±30	(13)
Eqn 36	1026	1027			1276		1127		(14)
Eqn 37	973	974			1262		1079		(14)
P_{NG85}	43	41.8	53.4	41.6	53.1	45.9	43.2	±5	(1)
P	42	40.8	49.7	40.2	52.4	41.5	41		(15)
$P_{Al\text{-}in\text{-}opx}$	43	41.4	53.7	40.5	57.7	42.3	41.6		(16)
P_{BBG08}	15.6	12.3	59.3	8.6	58	11.1	10		(17)
P_{NG85}	47.7	47.1	49.7	45.9	51.5	48	47.3		(18)
P_{RG96}	44.1	43	51	42	55	44.8	43.9		(19)
Eqn 38	11.9	12.9			12.9		18.9		(14)
Eqn 39	6.5	6.1			15.1		5.1		(14)

Reference sources: (1) Griffin et al. (2004); (2) Nimis and Grütter (2010); (3) Brey and Köhler (1990); (4) Canil (1999); (5) Ryan et al. (1996); (6) Canil (1994); (7) Griffin et al. (1989); (8) Harley (1984); (9) O'Neill and Wood (1979); *P = 30 kb; (10) Wu and Zhao (2007); (11) Ashchepkov (2006); (12–13) Brey and Köhler (1990); (14) Putirka (2008); (15) Finnerty and Boyd (1987); (16) Carswell (1991); (17) Brey et al. (2008); (18) Nickel and Green (1985); (19) Ryan et al. (1996).

provide enough time to achieve Mg isotopic equilibrium between garnet and olivine/opx.

5.2.2. Inter-mineral Fe isotopic fractionation

The isotopic compositions of Fe in minerals from the Kaapvaal garnet peridotites provide further insights into the evolution of the SCLM. Olivine has a slightly higher δ^{56}Fe than garnet, but similar δ^{56}Fe to opx (Fig. S5); this is consistent with observations from spinel peridotites, and reflects the controls of crystal structures on Fe isotopic fractionations (Williams et al., 2005; Zhao et al., 2010; Macris et al., 2015). As for the Mg isotopes, the observed $\Delta^{56}Fe_{olivine\text{-}opx}$ (-0.012 ± 0.047‰ to 0.042 ± 0.029‰) agree with theoretical predictions of inter-mineral equilibrium fractionation factors (-0.057‰ ~ -0.034‰ and -0.004‰ ~ -0.002‰) (Jackson et al., 2009; Dauphas et al., 2012, 2014) and (0.016‰–0.009‰) (Macris et al., 2015), respectively (Fig. 8), suggesting that Fe isotopes are also in equilibrium between olivine and opx.

Fe isotopic variations in mantle minerals do not vary significantly with depth in this study (Fig. 7). Previous studies have indicated that the distribution of Fe^{3+} between cpx and garnet in the garnet peridotites is strongly temperature-dependent; the Fe^{3+} in garnet increases markedly with increasing T and P, whereas that in cpx remains approximately constant (Luth et al., 1990; Canil and O'Neil, 1996). The garnet from high-T peridotites from greater depth is expected to have heavier Fe isotopic composition because ferric iron usually has higher δ^{56}Fe than ferrous iron (Polyakov et al., 2007; Schuessler et al., 2007; Shahar et al., 2008). However, this is not observed in our samples. Unlike Mg isotopes, there are no clear correlations between $\Delta^{56}Fe_{garnet\text{-}olivine/opx}$ and 1/T (Fig. 8d). Therefore, combined with the petrological systematics, garnet was probably not in Fe-isotope equilibrium with the coexisting minerals (olivine/opx/cpx) when they were captured by the kimberlites.

5.3. Mg- and Fe-isotope compositions of the deep upper mantle

Based on several different thermobarometers (Table 3), all coarse garnet peridotites analyzed here stem from a restricted pressure (depth) range of 4.2–5.3 GPa and a temperature range of 990 °C to 1191 °C (Fig. 2), plotting along the 40 mW/m^2 conductive geotherm of Chapman and Pollack (1977). The only deformed (sheared) garnet harzburgites (LT98/13) range from 1225 °C to 1413 °C at 5.2–5.8 GPa, in agreement with previous data (Finnerty and Boyd, 1987; Kennedy et al., 2002). Both suggest that these xenolith suites from Kaapvaal craton are derived from the thick lithospheric mantle with depths of 134–186 km.

5.3.1. Mg-isotope composition of garnet peridotites

δ^{26}Mg of garnet peridotite xenoliths in this study are shown in Fig. 3. JGF-98/6 has been extensively affected

Table 4
Mg-Fe isotopic fractionations among mantle minerals from the Kaapvaal craton.

Sample	LT98/3	LT98/5	LT98/10	LT98/12	LT98/13	LT98-14	LT98/15	JGF98/6
$\Delta^{26}Mg_{opx\text{-}olivine}$	0.019	−0.010	0.044	−0.006	−0.017	−0.022	0.032	0.048
2SD	0.040	0.040	0.042	0.040	0.032	0.043	0.021	0.060
$\Delta^{26}Mg_{cpx\text{-}olivine}$	0.027	−0.023			−0.041		−0.052	
2SD	0.035	0.032			0.035		0.034	
$\Delta^{26}Mg_{garnet\text{-}olivine}$	−0.410	−0.497	−0.317	−0.446	−0.299	−0.462	−0.450	
2SD	0.048	0.046	0.045	0.053	0.051	0.050	0.022	
$\Delta^{26}Mg_{garnet\text{-}opx}$	−0.429	−0.487	−0.366	−0.440	−0.282	−0.440	−0.482	
2SD	0.050	0.042	0.054	0.042	0.047	0.047	0.020	
$\Delta^{26}Mg_{garnet\text{-}cpx}$	−0.437	−0.474			−0.258		−0.398	
2SD	0.046	0.035			0.050		0.033	
$\Delta^{26}Mg_{cpx\text{-}opx}$	0.008	−0.013			−0.024		−0.084	
2SD	0.037	0.025			0.029		0.032	
$\Delta^{26}Mg_{olivine\text{-}phlogopite}$		−0.102						
2SD		0.046						
$\Delta^{56}Fe_{opx\text{-}olivine}$	−0.017	−0.042	−0.011	−0.014	0.012	−0.023	0.009	0.002
2SD	0.049	0.029	0.042	0.037	0.047	0.053	0.028	0.036
$\Delta^{56}Fe_{cpx\text{-}olivine}$	−0.042	−0.084			−0.004		−0.048	
2SD	0.054	0.018			0.043		0.026	
$\Delta^{56}Fe_{garnet\text{-}olivine}$	−0.150	−0.101	−0.056	−0.051	−0.024	−0.100	−0.060	
2SD	0.044	0.038	0.035	0.046	0.037	0.031	0.052	
$\Delta^{56}Fe_{garnet\text{-}opx}$	−0.132	−0.059	−0.045	−0.037	−0.037	−0.086	−0.070	
2SD	0.045	0.045	0.035	0.041	0.048	0.044	0.050	
$\Delta^{56}Fe_{garnet\text{-}cpx}$	−0.107	−0.017			−0.020		−0.013	
2SD	0.051	0.038			0.044		0.049	
$\Delta^{56}Fe_{cpx\text{-}opx}$	−0.025	−0.041			−0.017		−0.057	
2SD	0.055	0.031			0.052		0.021	
$\Delta^{56}Fe_{olivine\text{-}phlogopite}$		0.049						
2SD		0.062						

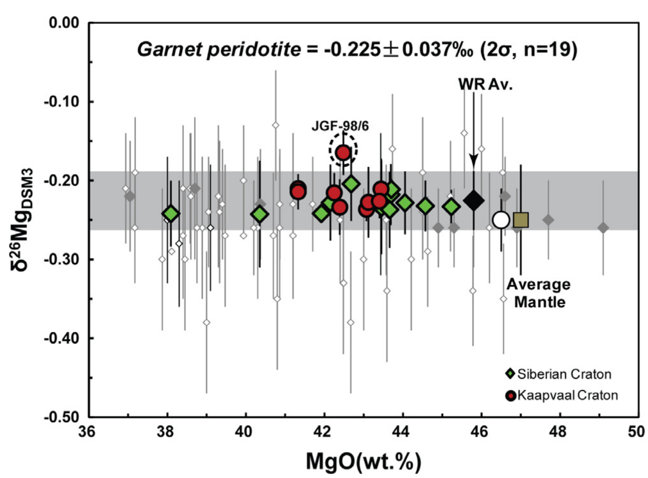

Fig. 3. δ^{26}Mg *vs* MgO (wt%) in garnet peridotites from the Kaapvaal and Siberian cratons. Large solid black diamond represents the average δ^{26}Mg of garnet peridotites analyzed in this study and the horizontal grey bar shows 2SD. Red circles and green diamonds represent the data for samples from the Kaapvaal and Siberian cratons, respectively. Solid square represents the Mg isotopic composition of Earth's mantle based on MORB, OIB, and peridotites in the literature (Bourdon et al., 2010; Teng et al., 2010a). Small open and solid diamonds represent the Mg isotopic compositions of spinel peridotites in the literature (Pogge von Strandmann et al., 2011; Xiao et al., 2013), and garnet peridotites from Northern Tanzania and off-craton garnet lherzolites from Vitim in southern Siberian, respectively (Teng et al., 2010; Pogge von Strandmann et al., 2011a). The white circle represents the average value of Mg isotopic compositions for spinel peridotites from the literature. (For interpretation of the references to colour in this figure legend, the reader is referred to the web version of this article.)

by metasomatism, which may have modified its isotopic composition. Therefore, it is not considered as a typical mantle rock here. The average δ^{26}Mg value of the other samples from Kaapvaal craton is $-0.221 \pm 0.034‰$ (2σ, $n = 7$), consistent with the average δ^{26}Mg of twelve garnet lherzolites from the central Siberian craton, $-0.230 \pm 0.039‰$ (2σ, $n = 12$). Therefore, we estimate that the lithospheric mantle has a δ^{26}Mg of $-0.225 \pm 0.037‰$ (2σ, $n = 19$), which is indistinguishable from the published δ^{26}Mg values for spinel-peridotite xenoliths, terrestrial

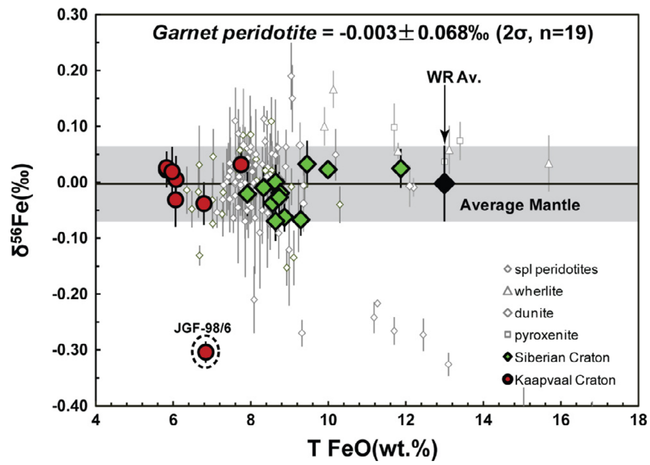

Fig. 4. δ^{56}Fe *vs* total FeO (wt%) in garnet peridotites from the Kaapvaal and Siberian cratons. Solid diamond and horizontal grey bar represent the average δ^{56}Fe and 2SD of garnet peridotites analyzed in this study. Small open symbols are δ^{56}Fe of different types of peridotites in the literature (Poitrasson et al., 2013; Schoenberg and Blanckenburg, 2006; Williams et al., 2005; Weyer et al., 2007; Zhao et al., 2015).

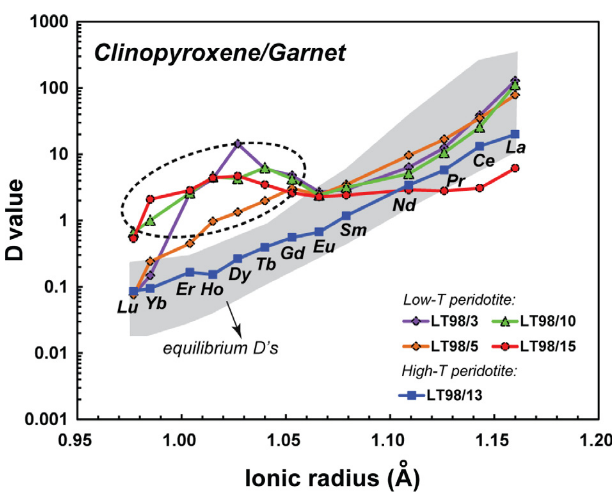

Fig. 5. Onuma diagram showing ${}^{cpx/garnet}D$ for trivalent cations entering the garnet X-site *vs* ionic radii of REE. Ionic radii are from Shannon (1976). The grey area indicates the experimentally-determined ${}^{cpx/garnet}D$ of REE from the literature (Harte and Kirkley, 1997; Green et al., 2000). Only the data for high-T peridotite (LT98/13, blue line) fall into the grey area. Although ${}^{cpx/garnet}D$ values of the LREE are consistent with equilibrium ones, the deviations of HREE from the theoretical results (dashed ellipse) indicate that the HREE are not in equilibrium between cpx and garnet in low-T coarse peridotites. This comparison shows that minerals crystallized during different episodes of metasomatism are characterized by trace-element disequilibrium.

komatiites, basalts, andesites, granodiorites, and chondrites in the literature (e.g., Bourdon et al., 2010; Dauphas et al., 2010; Teng et al., 2010a; Tipper et al., 2008a). There is no significant offset in the Mg isotopic composition between the shallow and deep upper mantle, and there has been no Mg isotopic fractionation during partial melting of deep mantle peridotites. Furthermore, neither degrees of partial melting (harzburgite *vs* primary lherzolite) nor the types of garnet peridotites (high-T deformed *vs* low-T coarse) in the ancient craton lithosphere can produce measurable Mg-isotopic variations in the deep upper mantle. The garnet peridotites from the SCLM, residues after large degrees (>30–50%) of melt extraction, show Mg isotopic compositions similar to the high-degree partial melts (~50%) from the mantle (e.g., komatiites), suggesting there is no resolvable Mg isotopic fractionation during partial melting of deep mantle peridotites and komatiite formation.

5.3.2. Fe-isotope composition of garnet peridotites

The δ^{56}Fe values of most whole rocks from these ancient cratons range from −0.069‰ to 0.060‰ (Fig. 4) with no clear Fe isotopic difference between the garnet peridotites from Kaapvaal and Siberian cratons. Excluding the obviously metasomatized sample (JGF-98/6), the average δ^{56}Fe of all whole rocks in this study is -0.003 ± 0.068‰ (2σ, $n = 19$). This value agrees well with those of previous studies on spinel and garnet peridotites (Williams et al., 2004, 2005; Weyer and Ionov, 2007; Poitrasson et al., 2013).

The deformed peridotite xenoliths with high equilibration temperatures and fertile compositions represent the SCLM altered by magma intruded from below, and they show extensive evidences of deformation and recrystallization with the formation of neoblasts (Gurney and Harte, 1980). The most important effect on the major elements was the introduction of Fe and Ti to these deformed peridotites (like LT98/13). However, there is no significant discrepancy in the δ^{56}Fe among different types of garnet peridotites in this study, regardless of FeO addition during later processes. Notably, the garnet peridotites with relatively high FeO contents (7.91–11.87 wt.%) from the Siberian craton also show similar Fe isotopic compositions to that from the Kaapvaal craton. In other words, the later metasomatic processes modified FeO contents of these whole rocks relative to the primitive mantle with 8.05 wt.% FeO (McDonough and Sun, 1995), but did not change the Fe isotopic compositions of the garnet lherzolites in this study (Fig. 4). Therefore, the lithospheric mantles under the Kaapvaal and Siberian cratons show homogeneous Fe isotopic compositions for garnet peridotites with depth from 134–186 km.

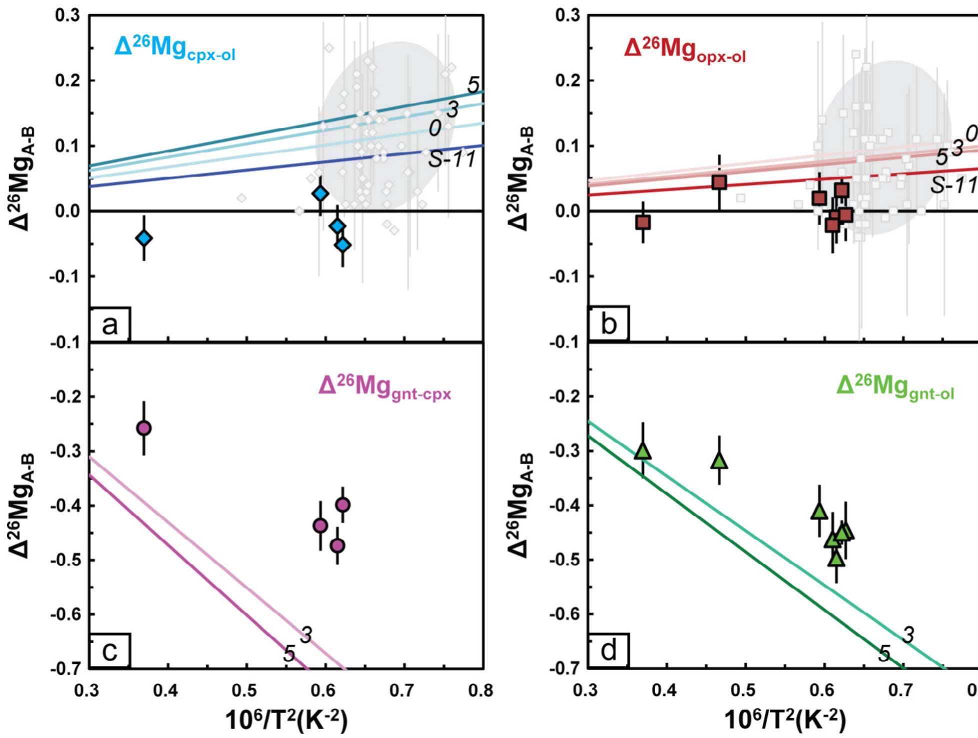

Fig. 6. Variations in Mg isotopic fractionation between mantle minerals with equilibration temperatures calculated using the Ca-in-Opx thermometer from Brey and Köhler (1990). The equilibrium isotopic-fractionation lines for Mg isotopes are from Schauble (2011) and Huang et al. (2013). Solid lines with numbers for $\Delta^{26}Mg_{garnet\text{-}cpx/olivine}$ and $\Delta^{26}Mg_{cpx/opx\text{-}olivine}$ represent equilibrium Mg isotopic fractionations under different pressures (0 GPa, 3 GPa, and 5 GPa). The cpx/opx-olivine data (S-11) are from Schauble (2011). The small open diamonds and squares enclosed by grey areas in (a) and (b) represent Mg isotopic fractionation among these minerals in spinel peridotites from the literature (Yang et al., 2009; Huang et al., 2011; Liu et al., 2011; Xiao et al., 2013).

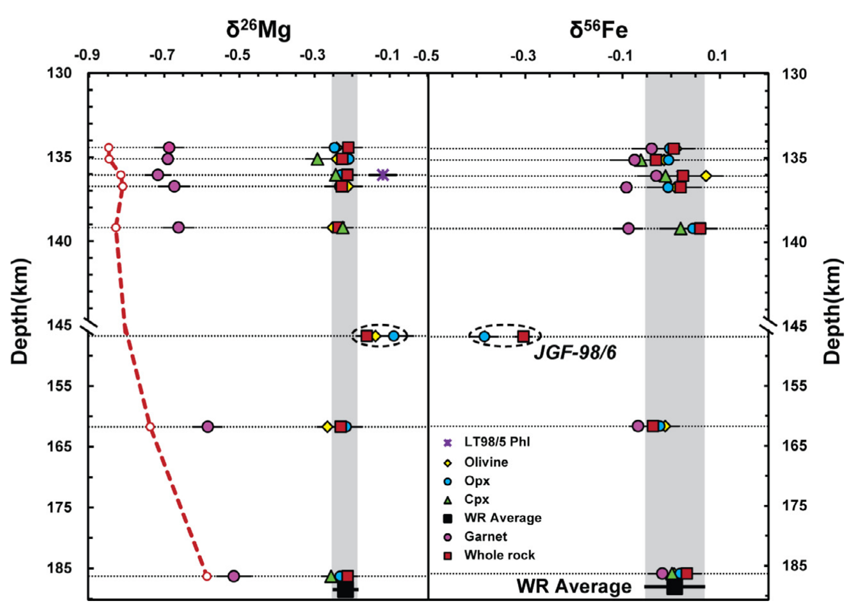

Fig. 7. Mg-Fe isotopic compositions of whole rocks and minerals as a function of depth (134–186 km) in the Kaapvaal craton. The grey areas represent the average Mg and Fe isotopic compositions of the whole rocks. There is a decrease in the extent of Mg isotopic fractionation between garnet and olivine/opx with increasing depth. However, these measured values are not consistent with equilibrium isotopic fractionations between garnet and olivine at the same depth (red dashed line). (For interpretation of the references to colour in this figure legend, the reader is referred to the web version of this article.)

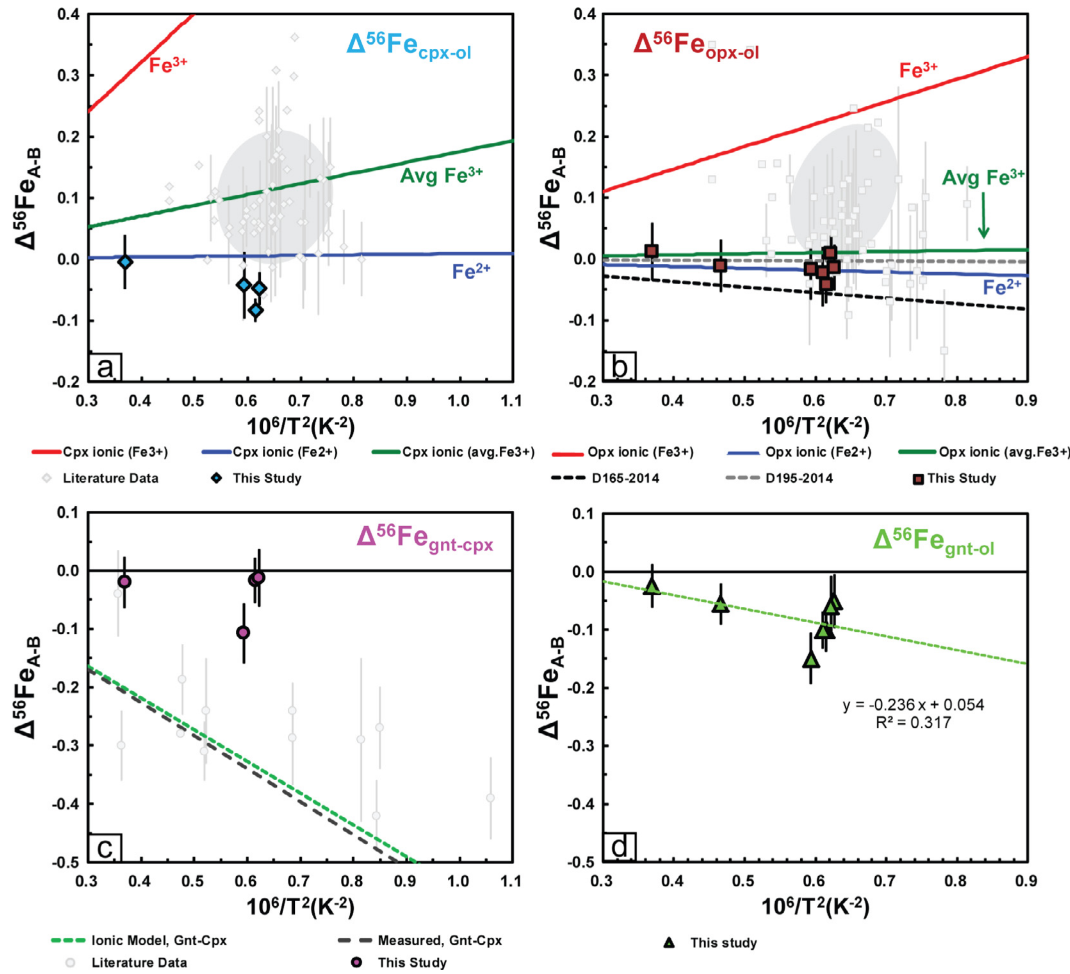

Fig. 8. Variations in Fe isotopic fractionation between mantle minerals *vs* equilibration temperatures calculated using the Ca-in-Opx thermometer from Brey and Köhler (1990). (a) and (b) Solid curves are ionic model calculations. All calculations are for Fe^{2+} only in olivine. (a) Lowermost solid curve (blue) is for all Fe^{2+} in cpx, uppermost solid curve (red) is for all Fe^{3+} in cpx, and the solid curve (green) in the middle is for average $Fe^{3+}/(Fe^{2+}+Fe^{3+}) = 0.2$ in cpx as reported by Macris et al. (2015). (b) The solid and dashed curves were calculated using ionic model and NRIXS data for two different opx compositions, respectively. Dashed curves are predictions from the NRIXS data for different force constants of Fe^{2+} in pyroxene (orthoenstatite, 165 N/m (black) to 195 N/m (grey)) (Jackson et al., 2009; Dauphas et al., 2012, 2014). The small open symbols enclosed by grey areas in (a) and (b) represent data of Fe isotopic fractionation among these minerals in spinel peridotites from the literature (Beard and Johnson, 2004; Zhao et al., 2010; Huang et al., 2011; Zhao et al., 2012; Zhao et al., 2015). (c) The temperature-dependent fractionation factors inferred from measurements of garnet-cpx from eclogite mantle xenoliths (Williams et al., 2009) are shown as the black dashed line and the ionic model garnet-cpx fractionation is shown as the green dashed line. Mantle xenolith garnet-cpx fractionations measured by Beard and Johnson (2004) are shown as small open circles. (d) There is no correlation of the Fe isotopic fractionation between garnet and olivine (dashed line) with equilibration temperature. (For interpretation of the references to colour in this figure legend, the reader is referred to the web version of this article.)

5.3.3. Variations of $\delta^{26}Mg$ and $\delta^{56}Fe$ in the deep upper mantle

Significant variation of $\delta^{56}Fe$ (from −0.309‰ to +0.060‰) has been observed for bulk peridotites between Jagersfontein and the other areas (N. Lesotho and Udachnaya) in this study. Sample JGF-98/6 has lower $\delta^{56}Fe$ (−0.309 ± 0.014‰) and slightly higher $\delta^{26}Mg$ (−0.168 ± 0.020‰) than other samples. Notably, CaO/Al_2O_3, $Mg^{\#}$, total FeO content, and the equilibration temperature of JGF-98/6 are not clearly different from other samples with normal $\delta^{26}Mg$ and $\delta^{56}Fe$ (Fig. S6), suggesting that the low $\delta^{56}Fe$ and high $\delta^{26}Mg$ values did not result from partial melting of the fertile mantle. Instead, the higher $^{187}Os/^{188}Os$ and La/Y of JGF-98/6 clearly indicate extensive metasomatic overprinting. This is similar to the previous observations on spinel peridotites and olivine minerals (Dauphas et al., 2010) with light Fe and slightly heavy Mg isotopic compositions. Therefore, we propose that the low $\delta^{56}Fe$ in JGF-98/6 could result from preferential diffusion of light Fe isotopes out of Fe-rich melt into the peridotite during melt percolation, a process similar to the E-2 type metasomatism (Weyer and Ionov, 2007; Zhao et al., 2010; Poitrasson et al., 2013). The bulk $\delta^{56}Fe$ of Kaapvaal peridotites shows a rough negative correlation with $\delta^{26}Mg$ (Fig. 9), a feature consistent with the prediction from theoretical modeling of isotopic fractionation in mantle miner-

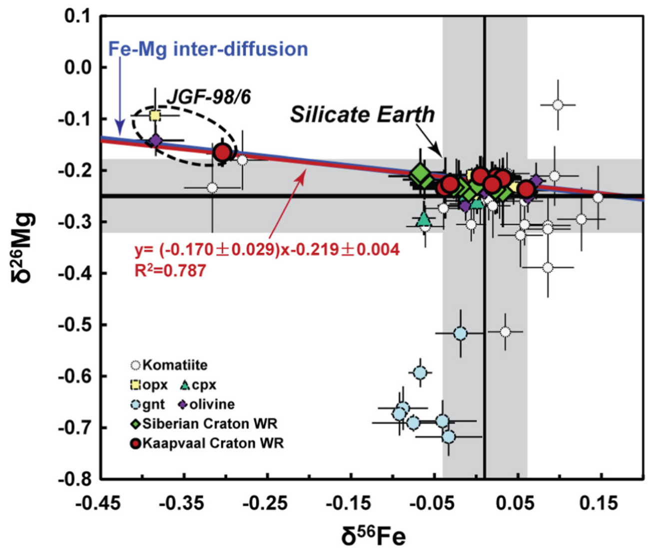

Fig. 9. δ^{56}Fe and δ^{26}Mg of olivine, opx, cpx, garnet, and bulk mantle peridotites. δ^{56}Fe shows a larger range than δ^{26}Mg, suggesting that the Fe isotopes of peridotites are more easily fractionated than Mg isotopes. Komatiite data are plotted for a comparison with peridotites (Dauphas et al., 2010). The negative correlation between δ^{56}Fe and δ^{26}Mg of all bulk rocks from the Kaapvaal craton was linearly fitted by a least-squared method (red line). Errors on slope and intercept reflect 2σ. The slope between δ^{56}Fe and δ^{26}Mg based on prediction from theoretical modeling is sensitive to the mass dependent isotopic fractionation factor (β) and relative abundances of Fe and Mg (or Mg#) in the peridotites. Variation of Mg and Fe isotopes can be constrained based on the equation in previous studies (e.g., $\frac{\delta^{56}Fe}{\delta^{26}Mg} \approx -\frac{\beta_{Fe}(56/54-1)Mg^{\#}}{\beta_{Mg}(26/24-1)(100-Mg)}$) (Dauphas et al., 2010). The slope of Fe-Mg inter-diffusion lines is −0.180 (blue line), which was calculated assuming $\beta_{Fe}/\beta_{Mg} = 1$ and $Mg^{\#} = 92.6$ (from JGF-98/6). (For interpretation of the references to colour in this figure legend, the reader is referred to the web version of this article.)

als or rocks due to Fe-Mg inter-diffusion (Dauphas et al., 2010). Finally, the metasomatic events responsible for the LREE enrichment (Grégoire et al., 2003) and phlogopite crystallization (Winterburn et al., 1990) in Jagersfontein should have not significantly modified the major-element compositions of sample JGF-98/6 (FeO = 6.84 wt.%) but produced obvious isotopic fractionation in the whole rock and minerals.

6. CONCLUSIONS

(1) The deep upper mantle (as represented by garnet peridotites) has similar Mg and Fe isotopic compositions ($\delta^{26}Mg = -0.225 \pm 0.037‰$; $\delta^{56}Fe = -0.003 \pm 0.068‰$, 2σ, $n = 19$) to spinel lherzolites, indicating that there is no significant Mg-Fe isotopic offset between the shallow and deep upper mantle.
(2) The similarity of Mg and Fe isotopic compositions between garnet peridotites and komatiites suggests a lack of significant Mg and Fe isotopic fractionation during partial melting of deep mantle peridotites and komatiite generation.
(3) $\Delta^{26}Mg_{garnet\text{-}olivine}$ and $\Delta^{26}Mg_{garnet\text{-}opx}$ decrease with increasing depth, reflecting the control of temperature and crystal structure on Mg isotopic fractionation. Olivine is in equilibrium with opx in terms of Fe and Mg isotopes, while garnet and cpx are not in equilibrium with the coexisting olivine and opx, reflecting melt-peridotite interaction during mantle metasomatism.

ACKNOWLEDGEMENT

This work was supported by the National Science Foundation of China (41603004, 41325011, 41173031, 40873009, and 41273045), the 111 Project, Anhui Provincial Natural Science Foundation (1608085QD74), and the Fundamental Research Funds for the Central Universities. The authors thank A. Galy for providing DSM-3 and CAM-1 standard solutions. We thank Weidong Sun for editorial handling and Paolo Sossi and an anonymous reviewer for the constructive comments. This is contribution 878 from the ARC Centre of Excellence for Core to Crust Fluid Systems (http://www.ccfs.mq.edu.au), and 1128 in the GEMOC Key Centre (http://www.gemoc.mq.edu.au).

APPENDIX A. SUPPLEMENTARY DATA

Supplementary data associated with this article can be found, in the online version, at http://dx.doi.org/10.1016/j.gca.2016.11.041.

REFERENCES

Agashev A. M., Ionov D. A., Pokhilenko N. P., Golovin A. V., Cherepanova Y. and Sharygin I. S. (2013) Metasomatism in lithospheric mantle roots: Constraints from whole-rock and mineral chemical composition of deformed peridotite xenoliths from kimberlite pipe Udachnaya. *Lithos* **160–161**, 201–215.
An Y., Wu F., Xiang Y., Nan X., Yu X., Yang J., Yu H., Xie L. and Huang F. (2014) High-precision Mg isotope analyses of low-Mg rocks by MC-ICP-MS. *Chem. Geol.* **390**, 9–21.
Ashchepkov I. V. (2006) Empirical garnet thermobarometer for mantle peridotites. *Russ. Geol. Geophys.* **47**, 1071–1085.

Ashchepkov I. V., Pokhilenko N. P., Vladykin N. V., Logvinova A. M., Afanasiev V. P., Pokhilenko L. N., Kuligin S. S., Malygina E. V., Alymova N. A., Kostrovitsky S. I., Rotman A. Y., Mityukhin S. I., Karpenko M. A., Stegnitsky Y. B. and Khemelnikova O. S. (2010) Structure and evolution of the lithospheric mantle beneath Siberian craton, thermobarometric study. *Tectonophysics* **485**, 17–41.

Ashchepkov I. V., Pokhilenko N. P., Vladykin N. V., Rotman A. Y., Afanasiev V. P., Logvinova A. M., Kostrovitsky S. I., Pokhilenko L. N., Karpenko M. A., Kuligin S. S., Malygina E. V., Stegnitsky Y. B., Alymova N. A. and Khmelnikova O. S. (2008) Reconstruction of mantle sections beneath Yakutian kimberlite pipes using monomineral thermobarometry. *Geol. Soc. Lond. Spec. Publ.* **293**, 335–352.

Baptiste V., Tommasi A. and Demouchy S. (2012) Deformation and hydration of the lithospheric mantle beneath the Kaapvaal craton, South Africa. *Lithos* **149**, 31–50.

Bascou J., Doucet L. S., Saumet S., Ionov D. A., Ashchepkov I. V. and Golovin A. V. (2011) Seismic velocities, anisotropy and deformation in Siberian cratonic mantle: EBSD data on xenoliths from the Udachnaya kimberlite. *Earth Planet. Sci. Lett.* **304**, 71–84.

Beard B. L. and Johnson C. M. (2004) Inter-mineral Fe isotope variations in mantle-derived rocks and implications for the Fe geochemical cycle. *Geochim. Cosmochim. Acta* **68**, 4727–4743.

Bell D. R., Schmitz M. D. and Janney P. E. (2003) Mesozoic thermal evolution of the southern African mantle lithosphere. *Lithos* **71**, 273–287.

Bourdon B., Tipper E. T., Fitoussi C. and Stracke A. (2010) Chondritic Mg isotope composition of the Earth. *Geochim. Cosmochim. Acta* **74**, 5069–5083.

Boyd F. R., Gurney J. J. and Richardson S. H. (1985) Evidence for a 150–200-km thick Archaean lithosphere from diamond inclusion thermobarometry. *Nature* **315**, 387–389.

Boyd F. R., Pokhilenko N. P., Pearson D. G., Mertzman S. A., Sobolev N. V. and Finger L. W. (1997) Composition of the Siberian cratonic mantle: evidence from Udachnaya peridotite xenoliths. *Contrib. Mineral. Petrol.* **128**, 228–246.

Brenot A., Cloquet C., Vigier N., Carignan J. and France-Lanord C. (2008) Magnesium isotope systematics of the lithologically varied Moselle river basin, France. *Geochim. Cosmochim. Acta* **72**, 5070–5089.

Brey G. P., Bulatov V. K. and Girnis A. V. (2008) Geobarometry for peridotites: experiments in simple and natural systems from 6 to 10 GPa. *J. Petrol.* **49**, 3–24.

Brey G. P. and Köhler T. (1990) Geothermobarometry in four-phase lherzolites II. New thermobarometers, and practical assessment of existing thermobarometers. *J. Petrol.* **31**, 1353–1378.

Burgess S. R. and Harte B. (2004) Tracing lithosphere evolution through the analysis of heterogeneous G9–G10 garnets in peridotite xenoliths, II: REE chemistry. *J. Petrol.* **45**, 609–633.

Canil D. (1994) An experimental calibration of the "Nickel in Garnet" geothermometer with applications. *Contrib. Mineral. Petrol.* **117**, 410–420.

Canil D. (1999) The Ni-in-garnet geothermometer: calibration at natural abundances. *Contrib. Mineral. Petrol.* **136**, 240–246.

Canil D. and O'Neil H. S. C. (1996) Distribution of ferric iron in some upper-mantle assemblages. *J. Petrol.* **37**, 609–635.

Carlson R. W., Boyd F. R., Shirey S. B., Janney P. E., GROVE T. L., Bowring S. A., Schmitz M. D., Dann J. C., Bell D., Gurney J. J., Richardson S. H., Tredoux M., Menzies A. H., Pearson D. G., Hart R. J., Wilson A. H. and Moser D. (2000) Continental growth, preservation, and modification in Southern Africa. *GSA Today* **10**, 1–7.

Carlson R. W., Pearson D. G. and James D. E. (2005) Physical, chemical, and chronological characteristics of continental mantle. *Rev. Geophys.* **43**.

Carswell D. A. (1991) The garnet-orthopyroxene Al barometer: problematic application to natural garnet lherzolite assemblages. *Mineral. Mag.* **55**, 19–31.

Chapman D. S. and Pollack H. N. (1977) Regional geotherms and lithospheric thickness. *Geology* **5**, 265–268.

Craddock P. R., Warren J. M. and Dauphas N. (2013) Abyssal peridotites reveal the near-chondritic Fe isotopic composition of the Earth. *Earth Planet. Sci. Lett.* **365**, 63–76.

Dauphas N., Craddock P. R., Asimow P. D., Bennett V. C., Nutman A. P. and Ohnenstetter D. (2009) Iron isotopes may reveal the redox conditions of mantle melting from Archean to Present. *Earth Planet. Sci. Lett.* **288**, 255–267.

Dauphas N., Roskosz M., Alp E. E., Golden D. C., Sio C. K., Tissot F. L. H., Hu M. Y., Zhao J., Gao L. and Morris R. V. (2012) A general moment NRIXS approach to the determination of equilibrium Fe isotopic fractionation factors: Application to goethite and jarosite. *Geochim. Cosmochim. Acta* **94**, 254–275.

Dauphas N., Roskosz M., Alp E. E., Neuville D. R., Hu M. Y., Sio C. K., Tissot F. L. H., Zhao J., Tissandier L., Médard E. and Cordier C. (2014) Magma redox and structural controls on iron isotope variations in Earth's mantle and crust. *Earth Planet. Sci. Lett.* **398**, 127–140.

Dauphas N., Teng F.-Z. and Arndt N. T. (2010) Magnesium and iron isotopes in 2.7 Ga Alexo komatiites: Mantle signatures, no evidence for Soret diffusion, and identification of diffusive transport in zoned olivine. *Geochim. Cosmochim. Acta* **74**, 3274–3291.

de Wit M. J., de Ronde C. E. J., Tredoux M., Roering C., Hart R. J., Armstrong R. A., Green R. W. E., Peberdy E. and Hart R. A. (1992) Formation of an Archaean continent. *Nature* **357**, 553–562.

Doucet L. S., Peslier A. H., Ionov D. A., Brandon A. D., Golovin A. V., Goncharov A. G. and Ashchepkov I. V. (2014) High water contents in the Siberian cratonic mantle linked to metasomatism: An FTIR study of Udachnaya peridotite xenoliths. *Geochim. Cosmochim. Acta* **137**, 159–187.

Eaton D. W., Darbyshire F., Evans R. L., Grütter H., Jones A. G. and Yuan X. (2009) The elusive lithosphere–asthenosphere boundary (LAB) beneath cratons. *Lithos* **109**, 1–22.

Finnerty A. and Boyd F. R. (1987) Thermobarometry for garnet peridotite xenoliths: basis for the determination of thermal and compositional structure of the upper mantle. In *Mantle Xenoliths* (ed. P. H. Nixon). Wiley, Chichester, pp. 381–402.

Frost D. J. and McCammon C. A. (2008) The redox state of Earth's mantle. *Annu. Rev. Earth Planet. Sci.* **36**, 389–420.

Galy A., Young E. D., Ash R. D. and Keith O'Nions R. (2000) The formation of chondrules at high gas pressures in the solar nebula. *Science* **290**, 1751–1753.

Goncharov A. G., Ionov D. A., Doucet L. S. and Pokhilenko L. N. (2012) Thermal state, oxygen fugacity and C-O-H fluid speciation in cratonic lithospheric mantle: New data on peridotite xenoliths from the Udachnaya kimberlite, Siberia. *Earth Planet. Sci. Lett.* **357–358**, 99–110.

Grégoire M., Bell D. and Le Roex A. (2002) Trace element geochemistry of phlogopite-rich mafic mantle xenoliths: their classification and their relationship to phlogopite-bearing peridotites and kimberlites revisited. *Contrib. Mineral. Petrol.* **142**, 603–625.

Grégoire M., Bell D. and Le Roex A. (2003) Garnet lherzolites from the Kaapvaal Craton (South Africa): trace element evidence for a metasomatic history. *J. Petrol.* **44**, 629–657.

Green T. H., Blundy J. D., Adam J. and Yaxley G. M. (2000) SIMS determination of trace element partition coefficients between garnet, clinopyroxene and hydrous basaltic liquids at 2–7.5 GPa and 1080–1200 °C. *Lithos* **53**, 165–187.

Griffin W. L., Cousens D. R., Ryan C. G., Sie S. H. and Suter G. F. (1989) Ni in chrome pyrope garnets: a new geothermometer. *Contrib. Mineral. Petrol.* **103**, 199–202.

Griffin W. L., Graham S., O'Reilly S. Y. and Pearson N. J. (2004) Lithosphere evolution beneath the Kaapvaal Craton: Re–Os systematics of sulfides in mantle-derived peridotites. *Chem. Geol.* **208**, 89–118.

Griffin W. L., Natapov L. M., O'Reilly S. Y., van Achterbergh E., Cherenkova A. F. and Cherenkov V. G. (2005) The Kharamai kimberlite field, Siberia: modification of the lithospheric mantle by the Siberian Trap event. *Lithos* **81**, 167–187.

Griffin W. L., O'Reilly S. Y., Natapov L. M. and Ryan C. G. (2003) The evolution of lithospheric mantle beneath the Kalahari Craton and its margins. *Lithos* **71**, 215–241.

Griffin W. L., Ryan C. G., Kaminsky F. V., O'Reilly S. Y., Natapov L. M., Win T. T., Kinny P. D. and Ilupin I. P. (1999b) The Siberian lithosphere traverse: mantle terranes and the assembly of the Siberian Craton. *Tectonophysics* **310**, 1–35.

Griffin W. L., Shee S. R., Ryan C. G., Win T. T. and Wyatt B. A. (1999d) Harzburgite to lherzolite and back again: metasomatic processes in ultramafic xenoliths from the Wesselton kimberlite, Kimberley, South Africa. *Contrib. Mineral. Petrol.* **134**, 232–250.

Griffin W. L., Smith D., Ryan C. G., O'Reilly S. Y. and Win T. T. (1996) Trace element zoning in mantle minerals metasomatism and thermal events in the upper mantle. *Can. Mineral.* **34**, 1179–1193.

Guillong M., Hametner K., Reusser E., Wilson S. A. and Gunther D. (2005) Preliminary characterisation of new glass reference materials (GSA-1G, GSC-1G, GSD-1G and GSE-1G) by laser ablation-inductively coupled plasma-mass spectrometry using 193 nm, 213 nm and 266 nm wavelengths. *Geostand. Geoanal. Res.* **29**, 315–331.

Gurney J. J. and Harte B. (1980) chemical variations in upper mantle nodules from Southern African Kimberlites.

Halicz L. and Gunther D. (2004) Quantitative analysis of silicates using LA-ICP-MS with liquid calibration. *J. Anal. At. Spectrom.* **19**, 1539–1545.

Handler M. R., Baker J. A., Schiller M., Bennett V. C. and Yaxley G. M. (2009) Magnesium stable isotope composition of Earth's upper mantle. *Earth Planet. Sci. Lett.* **282**, 306–313.

Harley S. (1984) An experimental study of the partitioning of Fe and Mg between garnet and orthopyroxene. *Contrib. Mineral. Petrol.* **86**, 359–373.

Harte B. and Kirkley M. B. (1997) Partitioning of trace elements between clinopyroxene and garnet: data from mantle eclogites. *Chem. Geol.* **136**, 1–24.

Hawkesworth C. J., Erlank A. J., Kempton P. D. and Waters F. G. (1990) Mantle metasomatism: Isotope and trace-element trends in xenoliths from Kimberley, South Africa. *Chem. Geol.* **85**, 19–34.

He Z., Huang F., Yu H., Xiao Y., Wang F., Li Q., Xia Y. and Zhang X. (2016) A flux-free fusion technique for rapid determination of major and trace elements in silicate rocks by LA-ICP-MS. *Geostand. Geoanal. Res.* **40**, 5–21.

Heimann A., Beard B. L. and Johnson C. M. (2008) The role of volatile exsolution and sub-solidus fluid/rock interactions in producing high 56Fe/54Fe ratios in siliceous igneous rocks. *Geochim. Cosmochim. Acta* **72**, 4379–4396.

Higgins J. A. and Schrag D. P. (2010) Constraining magnesium cycling in marine sediments using magnesium isotopes. *Geochim. Cosmochim. Acta* **74**, 5039–5053.

Hippler D., Buhl D., Witbaard R., Richter D. K. and Immenhauser A. (2009) Towards a better understanding of magnesium-isotope ratios from marine skeletal carbonates. *Geochim. Cosmochim. Acta* **73**, 6134–6146.

Huang F., Chakraborty P., Lundstrom C. C., Holmden C., Glessner J. J. G., Kieffer S. W. and Lesher C. E. (2010) Isotope fractionation in silicate melts by thermal diffusion. *Nature* **464**, 396–400.

Huang F., Chen L., Wu Z. and Wang W. (2013) First-principles calculations of equilibrium Mg isotope fractionations between garnet, clinopyroxene, orthopyroxene, and olivine: Implications for Mg isotope thermometry. *Earth Planet. Sci. Lett.* **367**, 61–70.

Huang F., Zhang Z., Lundstrom C. C. and Zhi X. (2011) Iron and magnesium isotopic compositions of peridotite xenoliths from Eastern China. *Geochim. Cosmochim. Acta* **75**, 3318–3334.

Huang J.-X., Xiang Y., An Y., Griffin W. L., Gréau Y., Xie L., Pearson N. J., Yu H. and O'Reilly S. Y. (2016) Magnesium and oxygen isotopes in Roberts Victor eclogites. *Chem. Geol.* **438**, 73–83.

Ionov D. A., Doucet L. S. and Ashchepkov I. V. (2010) Composition of the lithospheric mantle in the siberian craton: new constraints from fresh peridotites in the Udachnaya-east kimberlite. *J. Petrol.* **51**, 2177–2210.

Ionov D. A., Doucet L. S., Carlson R. W., Golovin A. V. and Korsakov A. V. (2015) Post-Archean formation of the lithospheric mantle in the central Siberian craton: Re–Os and PGE study of peridotite xenoliths from the Udachnaya kimberlite. *Geochim. Cosmochim. Acta* **165**, 466–483.

Ionov D. A., Doucet L. S. and Golovin A.V. (2013) The origin of garnet peridotites in the Siberian cratonic mantle from chemical, modal and textural data, Goldschmidt Abstract.

Jackson J. M., Hamecher E. A. and Sturhahn W. (2009) Nuclear resonant X-ray spectroscopy of (Mg, Fe)SiO_3 orthoenstatites. *Eur. J. Mineral.* **21**, 551–560.

Jaupart C. and Mareschal J. C. (1999) The thermal structure and thickness of continental roots. *Lithos* **48**, 93–114.

Jordan T. H. (1975) The continental tectosphere. *Rev. Geophys.* **13**, 1–12.

Kelemen P. B., Hart S. R. and Bernstein S. (1998) Silica enrichment in the continental upper mantle via melt/rock reaction. *Earth Planet. Sci. Lett.* **164**, 387–406.

Kennedy L. A., Russell J. K. and Kopylova M. G. (2002) Mantle shear zones revisited: The connection between the cratons and mantle dynamics. *Geology* **30**, 419–422.

Kobussen A. F., Griffin W. L. and O'Reilly S.Y. (2008b) The scale and scope of Cretaceous refertilisation of the Kaapvaal lithospheric mantle, Kaapvaal Craton, South Africa. In: 9th International kimberlite conference extended abstract 9IKC-A-00038.

Kobussen A. F., Griffin W. L. and O'Reilly S. Y. (2009) Cretaceous thermo-chemical modification of the Kaapvaal cratonic lithosphere, South Africa. *Lithos* **112**(Supplement 2), 886–895.

Kobussen A. F., Griffin W. L., O'Reilly S. Y. and Shee S. R. (2008a) Ghosts of lithospheres past: Imaging an evolving lithospheric mantle in southern Africa. *Geology* **36**, 515–518.

Krogh E. (1988) The garnet-clinopyroxene Fe-Mg geothermometer — a reinterpretation of existing experimental data. *Contrib. Mineral. Petrol.* **99**, 44–48.

Lazarov M., Woodland A. B. and Brey G. P. (2009) Thermal state and redox conditions of the Kaapvaal mantle: A study of xenoliths from the Finsch mine, South Africa. *Lithos* **112** (Supplement 2), 913–923.

Lee C.-T. A. (2005) Trace element evidence for hydrous metasomatism at the base of the North American lithosphere and possible association with laramide low-angle subduction. *J. Geol.* **113**, 673–685.

Li W.-Y., Teng F.-Z., Xiao Y. and Huang J. (2011) High-temperature inter-mineral magnesium isotope fractionation in eclogite from the Dabie orogen, China. *Earth Planet. Sci. Lett.* **304**, 224–230.

Liu S.-A., Teng F.-Z., Yang W. and Wu F.-Y. (2011) High-temperature inter-mineral magnesium isotope fractionation in mantle xenoliths from the North China craton. *Earth Planet. Sci. Lett.* **308**, 131–140.

Liu Y., Hu Z., Gao S., Günther D., Xu J., Gao C. and Chen H. (2008) In situ analysis of major and trace elements of anhydrous minerals by LA-ICP-MS without applying an internal standard. *Chem. Geol.* **257**, 34–43.

Luth R., Virgo D., Boyd F. and Wood B. (1990) Ferric iron in mantle-derived garnets. *Contrib. Mineral. Petrol.* **104**, 56–72.

Macris C. A., Manning C. E. and Young E. D. (2015) Crystal chemical constraints on inter-mineral Fe isotope fractionation and implications for Fe isotope disequilibrium in San Carlos mantle xenoliths. *Geochim. Cosmochim. Acta* **154**, 168–185.

McDonough W. F. and Sun S. S. (1995) The composition of the Earth. *Chem. Geol.* **120**, 223–253.

Misra K., Anand M., Taylor L. and Sobolev N. (2004) Multi-stage metasomatism of diamondiferous eclogite xenoliths from the Udachnaya kimberlite pipe, Yakutia, Siberia. *Contrib. Mineral. Petrol.* **146**, 696–714.

Nebel O., Sossi P. A., Bénard A., Wille M., Vroon P. Z. and Arculus R. J. (2015) Redox-variability and controls in subduction zones from an iron-isotope perspective. *Earth Planet. Sci. Lett.* **432**, 142–151.

Nickel K. G. and Green D. H. (1985) Empirical geothermobarometry for garnet peridotites and implications for the nature of the lithosphere, kimberlites and diamonds. *Earth Planet. Sci. Lett.* **73**, 158–170.

Nimis P. and Grütter H. (2010) Internally consistent geothermometers for garnet peridotites and pyroxenites. *Contrib. Mineral. Petrol.* **159**, 411–427.

Nimis P., Zanetti A., Dencker I. and Sobolev N. V. (2009) Major and trace element composition of chromian diopsides from the Zagadochnaya kimberlite (Yakutia, Russia): Metasomatic processes, thermobarometry and diamond potential. *Lithos* **112**, 397–412.

O'Neill H. C. and Wood B. J. (1979) An experimental study of Fe-Mg partitioning between garnet and olivine and its calibration as a geothermometer. *Contrib. Mineral. Petrol.* **70**, 59–70.

O'Reilly S. Y. and Griffin W. L. (2010) The continental lithosphere–asthenosphere boundary: Can we sample it? *Lithos* **120**, 1–13.

Pearson D. G., Canil D. and Shirey S. B. (2003) Mantle Samples Included in Volcanic Rocks: Xenoliths and Diamonds, in: Turekian, H.D.H.K. (Ed.). In *Treatise on Geochemistry* (eds. H. D. H. K. Turekian and R. W. Carlson). Pergamon, Oxford, pp. 171–276.

Pearson D. G., Carlson R. W., Shirey S. B., Boyd F. R. and Nixon P. H. (1995a) Stabilisation of Archaean lithospheric mantle: A Re-Os isotope study of peridotite xenoliths from the Kaapvaal craton. *Earth Planet. Sci. Lett.* **134**, 341–357.

Pearson D. G., Shirey S. B., Carlson R. W., Boyd F. R., Pokhilenko N. P. and Shimizu N. (1995b) Re-Os, Sm-Nd, and Rb-Sr isotope evidence for thick Archaean lithospheric mantle beneath the Siberian craton modified by multistage metasomatism. *Geochim. Cosmochim. Acta* **59**, 959–977.

Pogge von Strandmann P. A. E. (2008) Precise magnesium isotope measurements in core top planktic and benthic foraminifera. *Geochem. Geophys. Geosyst.* **9**, Q12015.

Pogge von Strandmann P. A. E., Elliott T., Marschall H. R., Coath C., Lai Y.-J., Jeffcoate A. B. and Ionov D. A. (2011) Variations of Li and Mg isotope ratios in bulk chondrites and mantle xenoliths. *Geochim. Cosmochim. Acta* **75**, 5247–5268.

Poitrasson F., Delpech G. and Grégoire M. (2013) On the iron isotope heterogeneity of lithospheric mantle xenoliths: implications for mantle metasomatism, the origin of basalts and the iron isotope composition of the Earth. *Contrib. Mineral. Petrol.* **165**, 1243–1258.

Polyakov V. B., Clayton R. N., Horita J. and Mineev S. D. (2007) Equilibrium iron isotope fractionation factors of minerals: Reevaluation from the data of nuclear inelastic resonant X-ray scattering and Mössbauer spectroscopy. *Geochim. Cosmochim. Acta* **71**, 3833–3846.

Polyakov V. B. and Mineev S. D. (2000) The use of Mössbauer spectroscopy in stable isotope geochemistry. *Geochim. Cosmochim. Acta* **64**, 849–865.

Poudjom Djomani Y. H., O'Reilly S. Y., Griffin W. L. and Morgan P. (2001) The density structure of subcontinental lithosphere through time. *Earth Planet. Sci. Lett.* **184**, 605–621.

Putirka K. D. (2008) Thermometers and barometers for volcanic systems. *Rev. Mineral. Geochem.* **69**, 61–120.

Rosen O. M., Condie K. C., Natapov L. M.and Nozhkin A.D. (1994) Archean and Early Proterozoic Evolution of the Siberian Craton: A Preliminary Assessment, in: Condie K. C. (Ed.), Developments in Precambrian Geology. Elsevier, Amsterdam, In: Condie K. C. (Ed.), Archean Crustal Evolution, pp. 411–459.

Rudnick R. L. and Nyblade A. A. (1999) The thickness and heat production of Archean lithosphere: constraints from xenoliths thermobarometry and surface heat flow. In: Fei Y. Bertka C. M. and Mysen, B. O. (Eds.), Mantle Petrology: Field observations and High-pressure Experimentation: Geochemical Society Special Publication 6, 3–12.

Ryan C. G., Griffin W. L. and Pearson N. J. (1996) Garnet geotherms: Pressure-temperature data from Cr-pyrope garnet xenocrysts in volcanic rocks. *J. Geophys. Res.: Solid Earth* **101**, 5611–5625.

Schauble E. A. (2011) First-principles estimates of equilibrium magnesium isotope fractionation in silicate, oxide, carbonate and hexaaquamagnesium(2+) crystals. *Geochim. Cosmochim. Acta* **75**, 844–869.

Schoenberg R. and Blanckenburg F. v. (2006) Modes of planetary-scale Fe isotope fractionation. *Earth Planet. Sci. Lett.* **252**, 342–359.

Schuessler J. A., Schoenberg R., Behrens H. and Blanckenburg F. v. (2007) The experimental calibration of the iron isotope fractionation factor between pyrrhotite and peralkaline rhyolitic melt. *Geochim. Cosmochim. Acta* **71**, 417–433.

Shahar A., Young E. D. and Manning C. E. (2008) Equilibrium high-temperature Fe isotope fractionation between fayalite and magnetite: An experimental calibration. *Earth Planet. Sci. Lett.* **268**, 330–338.

Shannon R. D. (1976) Revised effective ionic radii and systematic studies of interatomic distances in halides and chalcogenides. *Acta Crystallogr., Sect. A* **32**, 751–767.

Shatsky V., Ragozin A., Zedgenizov D. and Mityukhin S. (2008) Evidence for multistage evolution in a xenolith of diamond-bearing eclogite from the Udachnaya kimberlite pipe. *Lithos* **105**, 289–300.

Shimizu N. (1975) Rare earth elements in garnets and clinopyroxenes from garnet lherzolite nodules in kimberlites. *Earth Planet. Sci. Lett.* **25**, 26–32.

Shimizu N., Pokhilenko N. P., Boyd F. R. and Pearson D. G. (1997) Geochemical characteristics of mantle xenoliths from the Udachnaya kimberlite pipe. *Russ. Geol. Geophys.* **38**, 205–217.

Simon N. S. C., Carlson R. W., Pearson D. G. and Davies G. R. (2007) The origin and evolution of the Kaapvaal cratonic lithospheric mantle. *J. Petrol.* **48**, 589–625.

Simon N. S. C., Irvine G. J., Davies G. R., Pearson D. G. and Carlson R. W. (2003) The origin of garnet and clinopyroxene in "depleted" Kaapvaal peridotites. *Lithos* **71**, 289–322.

Skemer P. and Karato S.-I. (2008) Sheared lherzolite xenoliths revisited. *J. Geophys. Res.: Solid Earth* **113**.

Sleep N. H. (2003) Geodynamic implications of xenolith geotherms. *Geochem. Geophys. Geosyst.* **4**.

Smith C. B., Gurney J. J., Skinner E. M. W., Clement C. R. and Ebrahim N. (1985) Geochemical character of Southern African kimberlites; a new approach based on isotopic constraints. *S. Afr. J. Geol.* **88**, 267–280.

Stachel T., Aulbach S., Brey G. P., Harris J. W., Leost I., Tappert R. and Viljoen K. S. (2004) The trace element composition of silicate inclusions in diamonds: a review. *Lithos* **77**, 1–19.

Stachel T. and Harris J. W. (2008) The origin of cratonic diamonds — Constraints from mineral inclusions. *Ore Geol. Rev.* **34**, 5–32.

Stagno V., Ojwang D. O., McCammon C. A. and Frost D. J. (2013) The oxidation state of the mantle and the extraction of carbon from Earth/'s interior. *Nature* **493**, 84–88.

Stiefenhofer J. (1993) *The petrography, mineral chemistry and isotope geochemistry of a mantle xenolith suite from the Letlhakane DK 1 and DK 2 kimberlite pipes, Botswana*. Rhodes Univ., South Africa, Ph.D. Thesis.

Su B.-X., Teng F.-Z., Hu Y., Shi R.-D., Zhou M.-F., Zhu B., Liu F., Gong X.-H., Huang Q.-S., Xiao Y., Chen C. and He Y.-S. (2015) Iron and magnesium isotope fractionation in oceanic lithosphere and sub-arc mantle: Perspectives from ophiolites. *Earth Planet. Sci. Lett.* **430**, 523–532.

Teng F.-Z., Dauphas N., Helz R. T., Gao S. and Huang S. (2011) Diffusion-driven magnesium and iron isotope fractionation in Hawaiian olivine. *Earth Planet. Sci. Lett.* **308**, 317–324.

Teng F.-Z., Li W.-Y., Ke S., Marty B., Dauphas N., Huang S., Wu F.-Y. and Pourmand A. (2010) Magnesium isotopic composition of the Earth and chondrites. *Geochim. Cosmochim. Acta* **74**, 4150–4166.

Tipper E. T., Galy A. and Bickle M. J. (2008) Calcium and magnesium isotope systematics in rivers draining the Himalaya-Tibetan-Plateau region: Lithological or fractionation control? *Geochim. Cosmochim. Acta* **72**, 1057–1075.

Van Achterbergh E., Griffin W. and Stiefenhofer J. (2001) Metasomatism in mantle xenoliths from the Letlhakane kimberlites: estimation of element fluxes. *Contrib. Mineral. Petrol.* **141**, 397–414.

Walker R. J., Carlson R. W. and Shirey S. B. (1989) F.R., B., Os, Sr, Nd, and Pb isotope systematics of southern African peridotite xenoliths: Implications for the chemical evolution of subcontinental mantle. *Geochim. Cosmochim. Acta* **53**, 1583–1595.

Wasch L. J., van der Zwan F. M., Nebel O., Morel M. L. A., Hellebrand E. W. G., Pearson D. G. and Davies G. R. (2009) An alternative model for silica enrichment in the Kaapvaal subcontinental lithospheric mantle. *Geochim. Cosmochim. Acta* **73**, 6894–6917.

Weyer S., Anbar A. D., Brey G. P., Münker C., Mezger K. and Woodland A. B. (2005) Iron isotope fractionation during planetary differentiation. *Earth Planet. Sci. Lett.* **240**, 251–264.

Weyer S., Anbar A. D., Brey G. P., Münker C., Mezger K. and Woodland A. B. (2007) Fe-isotope fractionation during partial melting on Earth and the current view on the Fe-isotope budgets of the planets (reply to the comment of F. Poitrasson and to the comment of B.L. Beard and C.M. Johnson on "Iron isotope fractionation during planetary differentiation" by S. Weyer, A.D. Anbar, G.P. Brey, C. Münker, K. Mezger and A. B. Woodland). *Earth Planet. Sci. Lett.* **256**, 638–646.

Weyer S. and Ionov D. A. (2007) Partial melting and melt percolation in the mantle: The message from Fe isotopes. *Earth Planet. Sci. Lett.* **259**, 119–133.

Williams H. M., McCammon C. A., Peslier A. H., Halliday A. N., Teutsch N., Levasseur S. and Burg J.-P. (2004) Iron isotope fractionation and the oxygen fugacity of the mantle. *Science* **304**, 1656–1659.

Williams H. M., Nielsen S. G., Renac C., Griffin W. L., O'Reilly S. Y., McCammon C. A., Pearson N., Viljoen F., Alt J. C. and Halliday A. N. (2009) Fractionation of oxygen and iron isotopes by partial melting processes: Implications for the interpretation of stable isotope signatures in mafic rocks. *Earth Planet. Sci. Lett.* **283**, 156–166.

Williams H. M., Peslier A. H., McCammon C., Halliday A. N., Levasseur S., Teutsch N. and Burg J. P. (2005) Systematic iron isotope variations in mantle rocks and minerals: The effects of partial melting and oxygen fugacity. *Earth Planet. Sci. Lett.* **235**, 435–452.

Winterburn P. A., Harte B. and Gurney J. J. (1990) Peridotite xenoliths from the Jagersfontein kimberlite pipe: I. Primary and primary-metasomatic mineralogy. *Geochim. Cosmochim. Acta* **54**, 329–341.

Woodland A. B. and Koch M. (2003) Variation in oxygen fugacity with depth in the upper mantle beneath the Kaapvaal craton, Southern Africa. *Earth Planet. Sci. Lett.* **214**, 295–310.

Woolley A. R., Bergman S. C., Edgar A. D., Le Bas M. J., Mitchell R. H., Rock N. M. S. and Scott Smith B. H. (1996) Classification of lamprophyres, lamproites, kimberlites, and the kalsilitic, melilitic, and leucitic rocks. *Can. Mineral.* **34**, 175–186.

Wu C. M. and Zhao G. C. (2007) A recalibration of the garnet-olivine geothermometer and a new geobarometer for garnet peridotites and garnet-olivine-plagioclase-bearing granulites. *J. Metamorph. Geol.* **25**, 497–505.

Xiao Y., Teng F.-Z., Zhang H.-F. and Yang W. (2013) Large magnesium isotope fractionation in peridotite xenoliths from eastern North China craton: Product of melt–rock interaction. *Geochim. Cosmochim. Acta* **115**, 241–261.

Yang W., Teng F.-Z. and Zhang H.-F. (2009) Chondritic magnesium isotopic composition of the terrestrial mantle: A case study of peridotite xenoliths from the North China craton. *Earth Planet. Sci. Lett.* **288**, 475–482.

Yang W., Teng F.-Z., Zhang H.-F. and Li S.-G. (2012) Magnesium isotopic systematics of continental basalts from the North China craton: Implications for tracing subducted carbonate in the mantle. *Chem. Geol.* **328**, 185–194.

Yaxley G. M., Berry A. J., Kamenetsky V. S., Woodland A. B. and Golovin A. V. (2012) An oxygen fugacity profile through the Siberian Craton — Fe K-edge XANES determinations of Fe3+/$\sum$Fe in garnets in peridotite xenoliths from the Udachnaya East kimberlite. *Lithos* **140–141**, 142–151.

Young E. D., Manning C. E., Schauble E. A., Shahar A., Macris C. A., Lazar C. and Jordan M. (2015) High-temperature equilibrium isotope fractionation of non-traditional stable isotopes: Experiments, theory, and applications. *Chem. Geol.* **395**, 176–195.

Young E. D., Tonui E., Manning C. E., Schauble E. and Macris C. A. (2009) Spinel–olivine magnesium isotope thermometry in the mantle and implications for the Mg isotopic composition of Earth. *Earth Planet. Sci. Lett.* **288**, 524–533.

Zhao X.-M., Zhang H.-F., Zhu X.-K., Zhu B. and Cao H.-H. (2015) Effects of melt percolation on iron isotopic variation in peridotites from Yangyuan, North China Craton. *Chem. Geol.* **401**, 96–110.

Zhao X., Zhang H., Zhu X., Tang S. and Tang Y. (2010) Iron isotope variations in spinel peridotite xenoliths from North China Craton: implications for mantle metasomatism. *Contrib. Mineral. Petrol.* **160**, 1–14.

Zhao X., Zhang H., Zhu X., Tang S. and Yan B. (2012) Iron isotope evidence for multistage melt–peridotite interactions in the lithospheric mantle of eastern China. *Chem. Geol.* **292–293**, 127–139.

Zhu L. Y., Liu Y. S., Hu Z. C., Hu Q. H., Tong X. R., Zong K. Q., Chen H. H. and Gao S. (2013) Simultaneous determination of major and trace elements in fused volcanic rock powders using a hermetic vessel heater and LA-ICP-MS. *Geostand. Geoanal. Res.* **37**, 207–229.

Associate editor: Nicolas Dauphas